The effects of temperature, pH and redox state on the stability of glutamic acid in hydrothermal fluids

ARTICLE *in* GEOCHIMICA ET COSMOCHIMICA ACTA · JUNE 2014

Impact Factor: 4.33 · DOI: 10.1016/j.gca.2014.02.043

5 AUTHORS, INCLUDING:

Namhey Lee
Lawrence Berkeley National Laboratory
11 PUBLICATIONS **62** CITATIONS
SEE PROFILE

Robert M. Hazen
Carnegie Institution for Science
283 PUBLICATIONS **8,719** CITATIONS
SEE PROFILE

Available online at www.sciencedirect.com

ScienceDirect

Geochimica et Cosmochimica Acta 135 (2014) 66–86

Geochimica et Cosmochimica Acta

www.elsevier.com/locate/gca

The effects of temperature, pH and redox state on the stability of glutamic acid in hydrothermal fluids

Namhey Lee [a,b,*], Dionysis I. Foustoukos [b], Dimitri A. Sverjensky [a,b], George D. Cody [b], Robert M. Hazen [b]

[a] *Department of Earth and Planetary Sciences, Johns Hopkins University, Baltimore, MD 21218, USA*
[b] *Geophysical Laboratory, Carnegie Institution of Washington, Washington, DC 20015, USA*

Received 14 October 2013; accepted in revised form 26 February 2014; available online 13 March 2014

Abstract

Natural hydrothermal vent environments cover a wide range of physicochemical conditions involving temperature, pH and redox state. The stability of simple biomolecules such as amino acids in such environments is of interest in various fields of study from the origin of life to the metabolism of microbes at the present day. Numerous previous experimental studies have suggested that amino acids are unstable under hydrothermal conditions and decompose rapidly. However, previous studies have not effectively controlled the redox state of the hydrothermal fluids. Here we studied the stability of glutamate with and without reducing hydrothermal conditions imposed by 13 mM aqueous H_2 at temperatures of 150, 200 and 250 °C and initial (25 °C) pH values of 6 and 10 in a flow-through hydrothermal reactor with reaction times from 3 to 36 min. We combined the experimental measurements with theoretical calculations to model the *in situ* aqueous speciation and pH values. As previously observed under hydrothermal conditions, the main reaction involves glutamate cyclizing to pyroglutamate through a simple dehydration reaction. However, the amounts of decomposition products of the glutamate detected, including succinate, formate, carbon dioxide and ammonia depend on the temperature, the pH and particularly the redox state of the fluid. In the absence of dissolved H_2, glutamate decomposes in the sequence glutamate, glutaconate, α-hydroxyglutarate, ketoglutarate, formate and succinate, and ultimately to CO_2 and micromolar quantities of $H_{2(aq)}$. Model speciation calculations indicate the CO_2, formate and $H_{2(aq)}$ are not in metastable thermodynamic equilibrium. However, with 13 mM $H_{2(aq)}$ concentrations, the amounts of decomposition products are suppressed at all temperatures and pH values investigated. The small amounts of CO_2 and formate present are calculated to be in metastable equilibrium with the H_2. It is further proposed that there is a metastable equilibrium between glutamate, glutaconate, α-hydroxyglutarate, ketoglutarate and H_2. The key redox-sensitive step is the reaction of α-hydroxyglutarate to α-ketoglutarate, which is effectively inhibited by the elevated H_2 concentrations, which in turn dramatically lowers the amounts of all decomposition products including ammonia. Theoretical calculations of the metastable thermodynamic equilibrium between glutamate and ketoglutarate are consistent with the experimentally determined effects of reducing conditions. These findings establish that redox state is as important a variable as temperature and pH in affecting the stability of amino acids under hydrothermal conditions. It is suggested that when natural hydrothermal fluids contain enough dissolved H_2, the stability of amino acids may be enhanced in fluids at least on short time scales. In turn, this result suggests that reducing hydrothermal environments may have been favorable for assembling the building blocks of biomolecules in the origin of life. Furthermore, in present day hydrothermal vents the microbial ecosystems may in part be supported by the availability of metastable amino acids through heterotrophic metabolism.
Published by Elsevier Ltd.

* Corresponding author. Present address: Earth Science Division, Lawrence Berkeley National Laboratory, One Cyclotron Road, Berkeley, California 94720, USA. Tel.: +1 510 486 7466; Fax: 510-486-5686.
E-mail address: nlee@lbl.gov (N. Lee).

http://dx.doi.org/10.1016/j.gca.2014.02.043
0016-7037/Published by Elsevier Ltd.

1. INTRODUCTION

Since the discovery of hydrothermal vents at the Galapagos Rift in 1979 (Corliss et al., 1979), it has been suggested that the chemical evolution of biomolecules might have occurred in hydrothermal vent environments on the early Earth (Corliss and Hoffman, 1981; Shock, 1990b, 1992; Ferris, 1992; Amend and Shock, 1998; Huber and Wächtershäuser, 1998; Russell et al., 2005; Shock and Canovas, 2010). Hydrothermal origin-of-life theories have resulted in extensive studies of amino acids under such conditions (Bada and Miller, 1970; Bernhardt et al., 1984; White, 1984; Miller and Bada, 1988; Bada et al., 1995; Andersson and Holm, 2000; Cox and Seward, 2007a,b; Lemke et al., 2009). These studies have established that amino acids respond in different ways to hydrothermal conditions: some tend to break apart (e.g. Cox and Seward, 2007a,b) and others tend to polymerize or cyclize (Cleaves, 1950; Povoledo and Vallentyne, 1964; Vallentyne, 1964). It has also been recognized that mineral surfaces and the surfaces of the reactors used in experiments may have played a catalytic role in the breakdown of amino acids under hydrothermal conditions (Bada et al., 1995; Andersson and Holm, 2000; Cox and Seward, 2007a; Lemke et al., 2009). Overall, the previous experimental studies strongly suggest that amino acids are unstable under hydrothermal conditions.

Theoretical geochemical studies, however, have proposed that although amino acids are unstable under hydrothermal conditions with respect to decomposition to mixtures of CH_4 and CO_2, they may also exhibit a metastability that is of geochemical importance (Shock, 1990a,b, 1992, 2005; Shock and Canovas, 2010). At temperatures less than about 400 °C and pressures less than 1 kbar, abundant evidence from natural samples (Shock, 1988; Helgeson et al., 1993) and experiments (Seewald, 1994, 2001; McCollom and Seewald, 2003a,b; Foustoukos and Seyfried, 2004; Seewald et al., 2006) suggests that the formation of CH_4 in hydrothermal systems is kinetically inhibited without a mineral catalyst present. Under these circumstances, theoretical calculations predict that a rich variety of metastable aqueous organic carbon species can be expected (Manning et al., 2013). Theoretical calculations also predict that the most important variables in such systems are not only the temperature and pressure but also the redox state of the system (e.g. Shock and Canovas, 2010). The relative abundances of different organic molecules in hydrothermal systems are predicted to be a strong function of the redox state of the fluid, which in turn is manifested most obviously by the dissolved H_2.

Modern hydrothermal vent systems cover a wide range of physicochemical conditions, such as temperature, pressure, pH and redox state. A characteristic feature of many hydrothermal vent environments is the highly reducing redox state (relative to seawater) reflected by the elevated concentrations of aqueous H_2 produced by alteration of basalt or peridotite deep in the sub-seafloor reaction zone. This highly reducing condition results in hydrothermal fluids rich in the reduced aqueous species such as H_2S, Fe^{2+}, Mn^{2+}, Cu^{+}, NH_3 (Rona et al., 1983; Seyfried et al., 2004; Kelley et al., 2005; Foustoukos et al., 2008; Shock and Canovas, 2010). If the kinetic inhibition of methane redox equilibrium also occurs in these fluids, a great variety of metastable hydrothermal organic species may be formed (Shock, 1990a,b, 2005; Amend and Shock, 1998; Shock and Canovas, 2010). Analyses of the dissolved organic species in vent fluids have indicated a wide variety of organic species from light hydrocarbons such as methane through to heavy hydrocarbon species (Holm and Charlou, 2001; Proskurowski et al., 2008; Konn et al., 2009; Cruse and Seewald, 2010). Recently the possible existence of microbial communities that adopt heterotrophic metabolic processes supported by amino acids in sub-seafloor environments has been reported (Orsi et al., 2013).

Experimental studies of amino acid stabilities under hydrothermal conditions have so far rarely attempted to control the redox state of the systems being investigated. Notable exceptions include the studies of Hennet et al. (1992) and Andersson and Holm (2000). In both studies mineral assemblages were used to control the oxidation state of the system. However, the experiments were conducted at temperatures of 150 and 200 °C, respectively, likely too low to permit equilibrium between the minerals and aqueous solutions on the time scale of the experiments (54 h). Despite intensive efforts, we do not yet understand how organic molecules respond to high *T*–*P* conditions or how different environmental variables affect the molecules. However, experimental studies of hydrocarbons, organic acids and ketones (Seewald, 1994, 2001; McCollom and Seewald, 2003a,b; Yang et al., 2012), together with the theoretical calculations summarized above, have all demonstrated that metastable equilibrium exists and is a common feature of organic systems under hydrothermal conditions. It is clear that the role of redox and pH on the decomposition of amino acids dissolved in aqueous solutions should be investigated in order to understand the possible role of seawater hydrothermal circulation in the origin of life and the existence of microbial life in present-day mid-ocean ridge vent systems.

Here, we report results for the redox dependence of the glutamate decomposition under hydrothermal conditions. We investigate decomposition reaction pathways at a range of temperature and fluid pH conditions. We also include a kinetic analysis of glutamate conversion to pyroglutamate. Finally, we incorporate theoretical calculations modeling the *in situ* aqueous speciation and pH based on experimentally measured concentrations that enable us to examine the role of organic species metastable equilibria in the amino acid–NaOH–H_2O–H_2 system.

2. MATERIALS AND METHODS

2.1. Materials

All solutions were prepared with milli-Q water (Millipore resistance 17.9 Mega ohm). L-glutamic acid (Acros Organics, 99%) was used without any further purification. Reactant solutions were sonicated for at least 15 min and visually checked prior to use to ensure complete dissolution of glutamic acid. The pH was adjusted by adding precise

volumes of standardized NaOH in order to obtain the desired pH values. We measured the pH using a combination electrode (Thermo-Electron, Orion 8103 BNUWP) that was previously calibrated with standardized pH buffering solutions. Argon gas was constantly purged through the solution to avoid contamination by CO_2 from the air. The solution was kept under argon headspace. The entire flow-through system, including the titanium pressure vessel and tubing (oxidized Ti, Grade 5), were cleaned with 50% by volume HCl solution and deionized water prior to the experiment to remove organic contaminants. Further details of the experimental design adopted are presented in our next paper (Lee et al., in preparation).

2.2. Experimental setup

Experiments were performed by using two titanium flow-through cells configured in-series and by following procedures similar to those previously described (Foustoukos et al., 2011). Initially, glutamic acid solutions with adjusted pH were drawn into the pressure vessel (Fig. 1, Reaction cell #1). Once headspace was created, pressurized $H_{2(g)}$ was introduced into the vessel. Simultaneously, the solution was constantly agitated by a mixer to induce complete dissolution of $H_{2(aq)}$. Experimentally it was established that 500 psi of $H_{2(g)}$ will equilibrate with about 13 ± 1.8 mM of $H_{2(aq)}$ in less than 30 min at room temperature. Once a consistent concentration of $H_{2(aq)}$ was attained, the solution was delivered to the reactor cell (Reaction cell #2) located inside the oven. The reaction cell #2 has a fixed volume of 3.55 ml. It was placed inside a gravity-convection Lindberg/Blue oven with a temperature uniformity of 4 °C at 200 °C. Fluid delivery was facilitated by a high-precision dual-cylinder gas-tight titanium pump (Quizix SP5000) at constant flow rate of between 0.1 and 1.4 ml min^{-1}, while maintaining constant pressure conditions (140 bar) by an inline titanium backpressure regulator (Coretest DBPR-5). The connecting lines and reactor cells that go around the furnace were made of Ti-alloy and were pre-combusted in air to generate inert TiO_2 layers prior to the experiment. Samples were taken at different reaction times with gas-tight syringes. Dissolved gases and aqueous species were analyzed using gas chromatography, three different types of ionic chromatography and gas chromatography–mass spectrometry (GC–MS) for trace organic molecules. Considerable care has been taken to measure decomposition products quantitatively where possible.

2.3. Analytical methods

2.3.1. Ion chromatography for amino acid analysis

For the detection and measurement of amino acids and other anionic organic molecules a Dionex ICS-5000 AAA-Direct ionic chromatograph was used. The chromatograph was equipped with a 2-250 AminoPac PA10 analytical column and an integrated pulsed amperometry

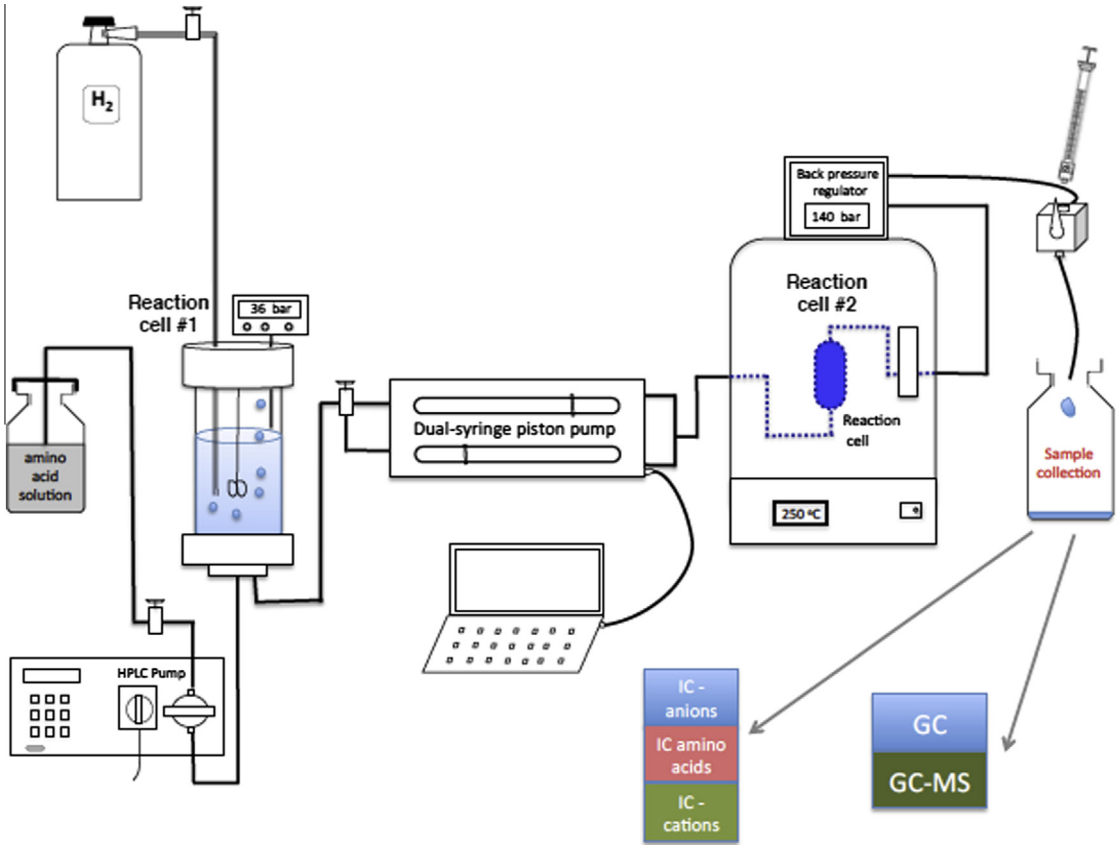

Fig. 1. Hydrothermal flow-through reactor with control of dissolved H_2.

(IPAD) electrochemical detector (Clarke et al., 1999). Unlike other traditional methods for analyzing amino acids, the AminoPac column allows the accurate detection of amino acids in water without the complications of pre- or post-column derivitization. The method consists of high-pH anion exchange separation of the analyte solution in the AminoPAC column followed by integrated pulsed amperometry electrochemical detection. Organic compounds that contain aliphatic amine groups are oxidized at the gold electrode in high pH condition which allows electrochemical detection of these molecules. Direct analysis of the amino acid used in this method not only minimizes the uncertainties of incomplete derivitization of conventional amino acid detection methods, but also allows monitoring for any additional amine-bearing decomposition products that formed during the hydrothermal experiments. Once the experimental samples were collected, they were kept frozen at −20 °C until analysis. We did experience problems of re-dissolving glutamate after it had precipitated during the freezing process. In order to ensure complete re-dissolution of the glutamate, it was essential to thaw the solutions and sonicate them for at least 15 min before analysis. In addition to being able to detect and analyze glutamate (and pyroglutamate), we checked for the presence of other possible amine-bearing species such as diglutamate or γ-aminobutyrate, but did not detect them. This result suggests that in the longest-reacted solutions, where the glutamate was at its lowest concentrations (about 100 μM), the concentrations of these possible reaction products were under detection limit (∼0.1 μM).

2.3.2. Ion chromatography for aliphatic acid and pyroglutamate analysis

Aliphatic decomposition products such as formate were analyzed with a Metrohm MIC-3 Advanced ionic chromatograph equipped with a Metrosep A sup 7-250 column and conductivity detector. Pyroglutamate, the major product in the experiments was analyzed in this way. Formate was also measured quantitatively. Different dilution factors were used for each molecule. The possible production of additional anions by decomposition of glutamate was also monitored. No peaks were observed for acetate, acetone, glyoxylate and propionate, which suggest that the concentration of these species were below detection limits.

2.3.3. Cation chromatography for ammonium analysis

After acidification of the fluid samples, decomposition products that can be cationic such as ammonium ion were also monitored and analyzed with the Dionex ion chromatograph ICS-5000 using a 250 IonPac CS12A analytical column and conductivity detector. With the exception of Na^+ and NH_4^+, no other cations were detected.

2.3.4. Gas chromatography for dissolved gaseous species

Gaseous species were analyzed with a Shimadzu GC-8A gas chromatograph equipped with a thermal conductivity detector and a Carboxeen-1010 Plot/Silica Gel column. The detection limit on these volatiles is 1–5 μM with analytical errors (2σ within about 10%. For dissolved gas analysis, the sample fluids were collected in gas-tight Teflon-glass Hamilton locking syringes. The fluid sample was collected in a pre-acidified syringe to ensure the complete conversion of dissolved carbonated species into $CO_{2(g)}$ followed by headspace extraction of the sample syringe with Ar gas. The products of glutamate decomposition measured in this way were total dissolved ΣCO_2 (which represented $CO_{2(aq)} + HCO_3^- + CO_3^{2-}$) and $H_{2(aq)}$. Within our given times of reaction we did not detect $CH_{4(aq)}$ or CO, suggesting that the concentrations of these species were probably below the detection limit.

2.3.5. Gas chromatography-mass spectroscopy (GC–MS)

Gas chromatography-mass spectroscopy (GC–MS) was used on selected samples to detect trace amounts of decomposition products. The machine used was an Agilent – 6890N Gas Chromatograph–Mass Spectrometer. First, sample aliquots were dried on a hot plate to remove water and to yield dried masses of ∼0.1 mg. Then the hydroxyl groups were derivatized using MTBSTFA (*N*-(tert-butyldimethylsilyl)-*N*-methyltrifluoroacetamide) and acetotrile. The samples were allowed to react overnight at 60 °C on a hot plate and the next day were diluted with dichloromethane (DCM) and analyzed. Using this method, we were able to identify succinate, glutaconate and α-hydroxyglutarate. We investigated the possibility of β-hydroxyglutarate formation, however, all of the hydroxyglutarate detected was exclusively in the α-form. We also analyzed the stock glutamic acid to monitor the concentrations of organic contaminants. This test confirmed that the organic molecules identified were formed in the course of the experiments, not from impurities in the stock chemicals.

We also report the succinic acid produced at the longest reaction time at different redox states. The analyses were replicated at least twice. We experienced different yields of derivatization of succinic acid as a function of pH. This is due to the fact that at high pH, succinic acid forms a Na-succinate complex, which inhibits facile derivatization (Lee et al., in preparation). Therefore, the reported concentrations of succinic acid at high pH are only minimum values.

3. RESULTS AND DISCUSSION

3.1. Conversion of glutamate into pyroglutamate

Glutamic acid under high-temperature conditions spontaneously cyclizes via a dehydration reaction forming a 5-member ring according to:

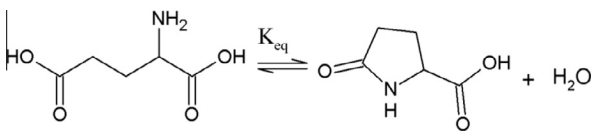

Table 1
Measured experimental concentrations of dissolved species in experiments conducted at 140 bar. The symbol "–" indicates concentrations that were below detection limits.

	T (min)	Glutamate (mM)	Pyroglutamate (mM)	Formate (μM)	$CO_{2(aq)}$ (mM)	$H_{2(aq)}$ (μM)	NH_4^+ (μM)
(a)							
No H_2 added initial $pH_{25\,°C}$ 10	3.55	9.33	0.32	–	0.00	0.00	–
$T = 150$ °C							
	3.55	9.34	0.32	–	0.10	0.01	–
	3.55	9.36	0.32	–	0.12	0.01	–
	7.10	8.99	0.68		0.06	0.01	–
	7.10	8.99	0.68	–	0.15	0.00	–
	7.10	8.98	0.69	–	0.20	0.01	–
	11.83	8.20	1.47	–	0.10	0.01	–
	11.83	8.17	1.50	–	0.09	0.01	–
	11.83	8.16	1.48	–	0.15	0.01	–
	35.5	4.71	4.95	20.00	0.10	0.01	–
	35.5	4.76	4.90	15.00	0.23	0.01	–
	35.5	4.61	5.06	16.00	0.08	0.01	–
(b)							
No H_2 added initial $pH_{25°C}$ 6	2.54	8.97	0.66	–	0.07	1.22	–
$T = 200$ °C							
	2.54	8.79	0.65	–	0.07	2.17	–
	2.54	8.87	0.67	–	0.08	1.09	–
	3.55	7.91	1.46	–		1.40	–
	3.55	7.61	1.46	–	0.12	1.16	–
	3.55	8.17	1.47	–	0.09	0.74	–
	4.4	6.64	2.68	–	0.11	1.46	10.06
	4.4	6.54	0.53	–	0.07	2.27	9.00
	4.4	6.59	2.77	–	0.07	1.59	9.89
	7.10	2.97	6.40		0.11	1.81	67.47
	7.10	3.15	6.21	6.99	0.15	2.22	66.35
	7.10	3.01	6.21	6.11	0.21	2.03	66.07
	11.83	0.94	8.57	6.57	0.19	2.46	90.53
	11.83	0.94	8.13	7.00	0.21	2.35	94.22
	11.83	0.88	8.45	6.75	0.22	2.47	90.81
	35.5	0.36	9.17	7.63	0.14	3.80	73.07
	35.5	0.35	9.18	6.89	0.16	3.53	68.31
	35.5	0.36	9.26	7.93	0.16	3.21	69.71
(c)							
H_2-enriched solution initial $pH_{25\,°C}$ 6	2.54	0.76	9.84	–	0.01	17.64	11.06
$T = 200$ °C							
	2.54	0.77	10.11	–	0.01	15.01	11.24
	2.54	0.80	10.47	–	0.05	18.23	10.83
	3.55	1.62	9.57	–	0.06	13.34	7.49
	3.55	1.63	9.61	–	0.04	11.73	–
	3.55	1.63	9.07	–	0.03	15.95	–
	4.4	2.77	7.80	–	0.05	14.85	–
	4.4	2.74	7.62	–	0.02	10.20	–
	4.4	2.73	7.68	–	0.04	17.94	–
	7.10	6.67	3.31		0.03	17.23	–
	7.10	6.71	3.32	6.99	0.03	14.26	–
	7.10	6.69	3.40	6.11	0.05	13.69	–
	2.54	8.96	0.32	6.57	0.05	20.84	–
	2.54	9.07	0.28	7.00	0.05	17.14	–
	2.54	9.08	0.28	6.75	0.04	19.52	–
	35.5	9.74	0.07	7.63	0.07	16.49	–
	35.5	9.77	0.09	6.89	0.02	16.28	–
	35.5	9.78	0.09	7.93	0.04	15.61	–
$T = 250$ °C	2.54	3.78	6.39	7.10	0.016	9.5	44.6
	2.54	3.74	6.24	7.07	0.036	12.9	44.0
	2.54	4.18	6.27	7.09	0.064	15.5	45.0
	3.01	0.95	8.58	7.07	0.092	10.8	25.7
	3.01	1.02	8.60	7.07	0.062	11.6	25.4

(*continued on next page*)

Table 1 (*continued*)

T (min)	Glutamate (mM)	Pyroglutamate (mM)	Formate (μM)	$CO_{2(aq)}$ (mM)	$H_{2(aq)}$ (μM)	NH_4^+ (μM)
3.01	1.00	8.61	7.06	0.049	15.8	25.2
3.55	0.57	9.36	7.09			
3.55	0.53	9.37	7.05	0.070	11.3	27.9
3.55	0.52	9.49	7.04	0.079	13.5	29.8
7.1	0.40	9.55	15.68	0.147	13.9	19.6
7.1	0.42	9.64	16.11	0.109	12.3	19.3
7.1	0.37	9.57	16.19	0.066	15.6	19.3
11.83	0.41	9.60	21.36	0.070	13.1	17.3
11.83	0.46	9.68	24.33	0.087	11.9	17.7
11.83	0.49	9.60	24.65	0.067	12.8	17.7
35.5	0.44	9.56	28.73	0.084	18.4	19.2
35.5	0.40	9.53	28.92	0.041	19.1	18.5
35.5	0.43	9.56	29.41	0.063	15.6	18.5

In this reaction, the side chain carboxylic group of the glutamate loses its –OH, which combines with a proton from the amine group forming water, leaving an amide group on the pyroglutamate. The reaction is reversible but does not occur readily at room temperature. The product molecule pyroglutamate is known to be more heat resistant than glutamate, suggesting a protective mode for the glutamic acid under high-temperature conditions (Povoledo and Vallentyne, 1964). This phenomenon has been reported in previous studies in the protein analysis and biomedical communities (Wilson and Cannon, 1937; Cleaves, 1950; Povoledo and Vallentyne, 1964). However, quantitative kinetic information has been lacking. Here we report the kinetics of the cyclization reaction of glutamate at varying temperature, pH and redox conditions.

The temperatures studied were 150, 200 and 250 °C. At each temperature, samples were collected at 4–6 different reaction times ranging from 3 to 36 min (Table 1). For example, Fig. 2 shows the measured concentrations of glutamate and pyroglutamate produced at each reaction time at different temperatures in one set of the H_2-free experiments. Here, it can be seen that at 150 °C the conversion of glutamate to pyroglutamate occurs approximately linearly with time. At this temperature, after ~36 min of reaction, approximately 63% of the glutamate is converted to pyroglutamate. At 200 °C, the initial linear correlation between the dissolved species is shorter (~7 min), and the glutamate appears to reach a steady state with pyroglutamate in about 15 min. At 250 °C, the conversion reaction occurs even faster, reaching a steady state in less than 5 min.

The reaction in Eq. (1) is a simple dehydration reaction and is not expected to depend on the redox state or pH of the system, i.e. the ratio of pyroglutamate to glutamate at a given temperature and pressure should be independent of other variables. The results are plotted as logarithmic ratios of pyroglutamate to glutamate as a function of reaction time (Fig. 3). It can be seen in Fig. 3a that the ratio of pyroglutamate to glutamate progressively increases and apparently at this low temperature does not reach a steady state value. However, with the exception of the upper curve at 200 °C and initial $pH_{25\,°C}$ of 6 (Fig. 3d), the ratio of pyroglutamate

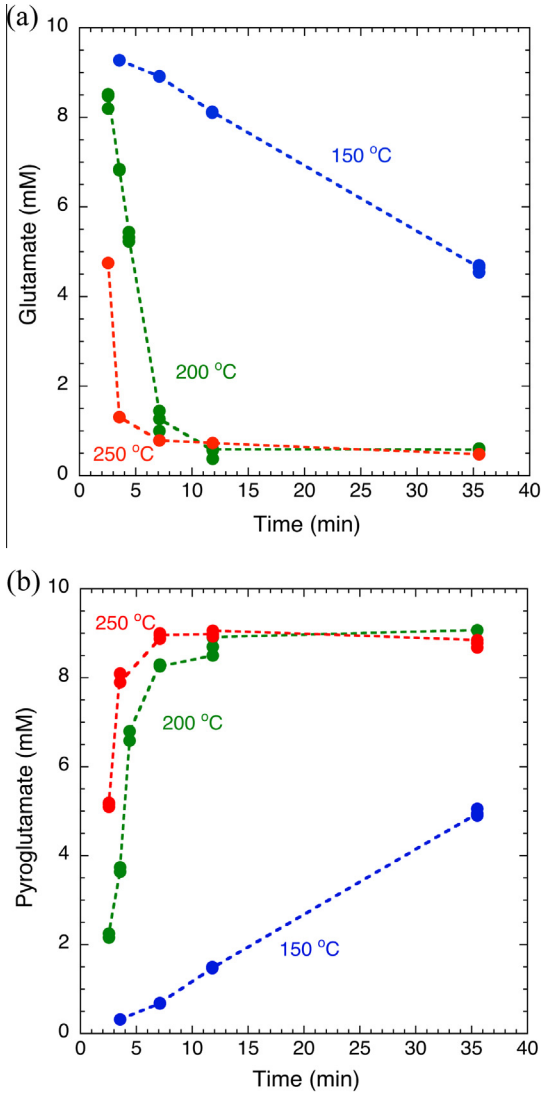

Fig. 2. Concentration changes of glutamate (a) and pyroglutamate (b) with reaction time corresponding to initial $pH_{25\,°C} = 10$ with no H_2 added.

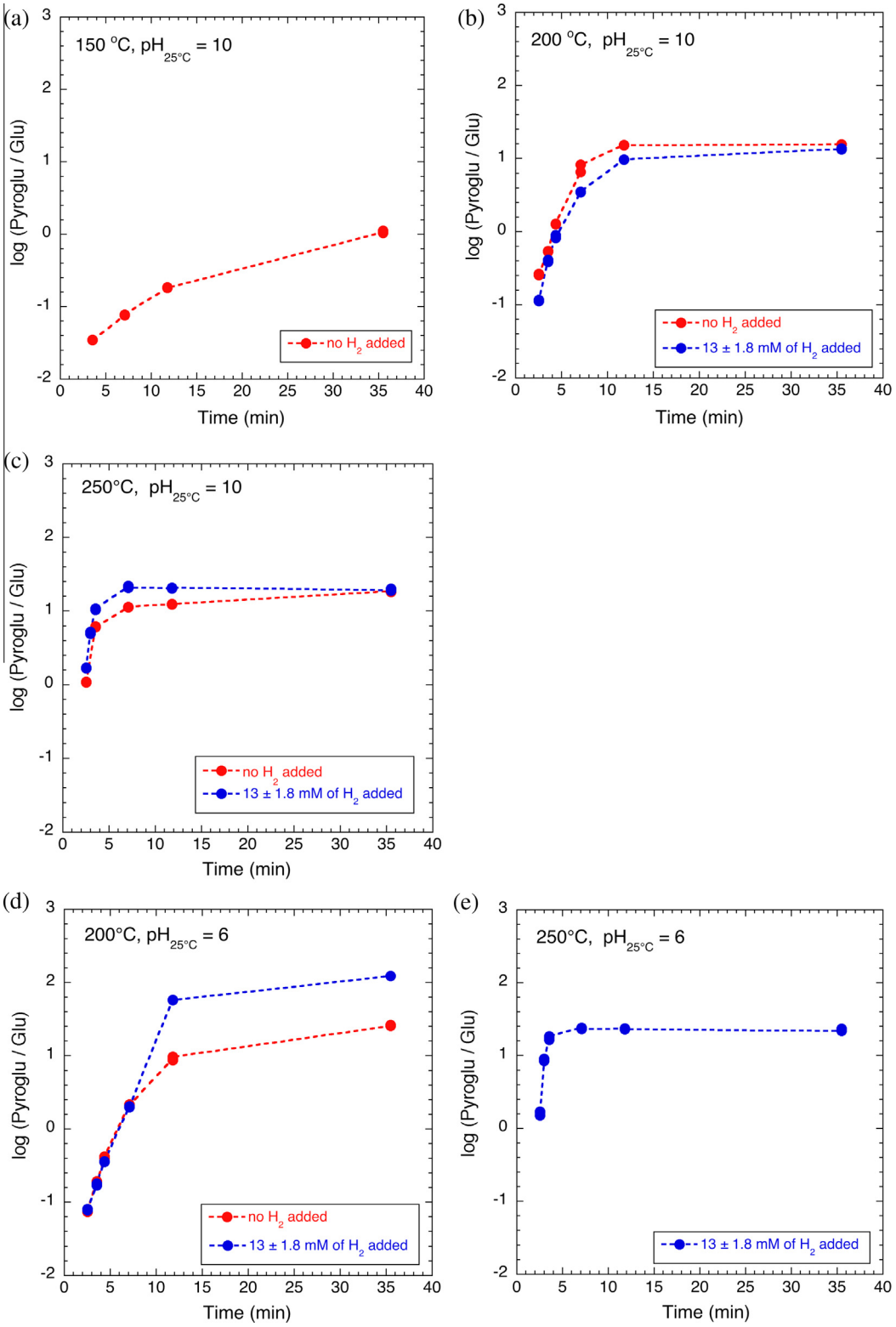

Fig. 3. Logarithmic ratio of pyroglutamate and glutamate versus reaction time: (a) 150 °C, no H_2 added; (b) at 250 °C, initial $pH_{25°C}$ 6 with and without H_2 added; (c) at 200 °C, initial $pH_{25°C}$ 10 with and without H_2 added; and (d) at 200 °C, initial $pH_{25°C}$ 6 with and without H_2 added.

to glutamate is approximately constant with a value of about 1.0 to 1.4 at the longest reaction times as expected (Fig. 3b–e). Small discrepancies may be attributed to uncertainties in measuring small quantities of glutamate relative to large quantities of pyroglutamate. An alternative explanation is that if small amounts of glutamate and/or pyroglutamate decompose to different extents depending on the redox state, it is possible that the final values of glutamate and pyroglutamate concentrations could be lower than otherwise.

3.1.1. Kinetics of conversion as a function of temperature

Assuming that the reaction of glutamate to pyroglutamate is pseudo first-order, we can express the conversion by the equation

$$-\frac{dm_{Glutamate}}{dt} = k_{glu} \cdot m_{Glutamate} \quad (1)$$

where $m_{Glutamate}$ represents the molality of glutamate, and k_{glu} is the rate coefficient for glutamate conversion in s^{-1} and t represents time in seconds. We applied Eq. (1) only to the rapidly changing far-from equilibrium experimental data in Fig. 3 (referring to an initial $pH_{25\,°C}$ of 10) and assuming that the redox state does not affect the kinetics as discussed above.

Fig. 4(a) shows the natural logarithmic ratios of glutamate normalized to the initial glutamic acid concentration at each reaction time and temperature. At each temperature, an initial linear relationship is observed, in good agreement with the assumption of a first-order reaction. This enables extraction of the kinetic rate coefficients (k_{glu}) described as the slope of the linear relationships between ln ($Glu/Glu_{initial}$) and reaction time (min). It is observed that with increasing temperature from 150 to 250 °C, the estimated values of k_{glu} increase by roughly one order of magnitude for each 50 °C temperature increment (Table 2). The reaction rate coefficients can be also expressed as half-lives ($t_{1/2}$) that are independent of the starting concentration for first-order kinetics (Fig. 4b):

$$t_{\frac{1}{2}} = \frac{\ln(2)}{k} \quad (2)$$

The half-life was calculated to be about 40 min at 150 °C, 2.4 min at 200 °C and 0.5 min at 250 °C (Table 2).

The observed rate coefficients can also be related to the temperature using the Arrhenius equation defined as follows:

$$\ln(k_{glu}) = \ln(A) - \frac{E_a}{RT} \quad (3)$$

where E_a is the activation energy, T is the temperature in Kelvin and A is a pre-exponential factor (s^{-1}) and R is the universal gas constant (8.314 J mol^{-1} K^{-1}). For the glutamate to pyroglutamate conversion, the linear temperature dependence of the reaction coefficient showed an excellent agreement with the Arrhenius equation (Fig. 4c), yielding an estimated activation energy and pre-exponential factor corresponding to 86 ± 0.63 kJ mol^{-1} and $1.3 \times 10^7 \pm 2.4 \times 10^6$ s^{-1}, respectively (Table 2).

3.2. Decomposition products of glutamate/pyroglutamate

Formation of pyroglutamate helps the survivability of glutamic acid under hydrothermal conditions. Nevertheless,

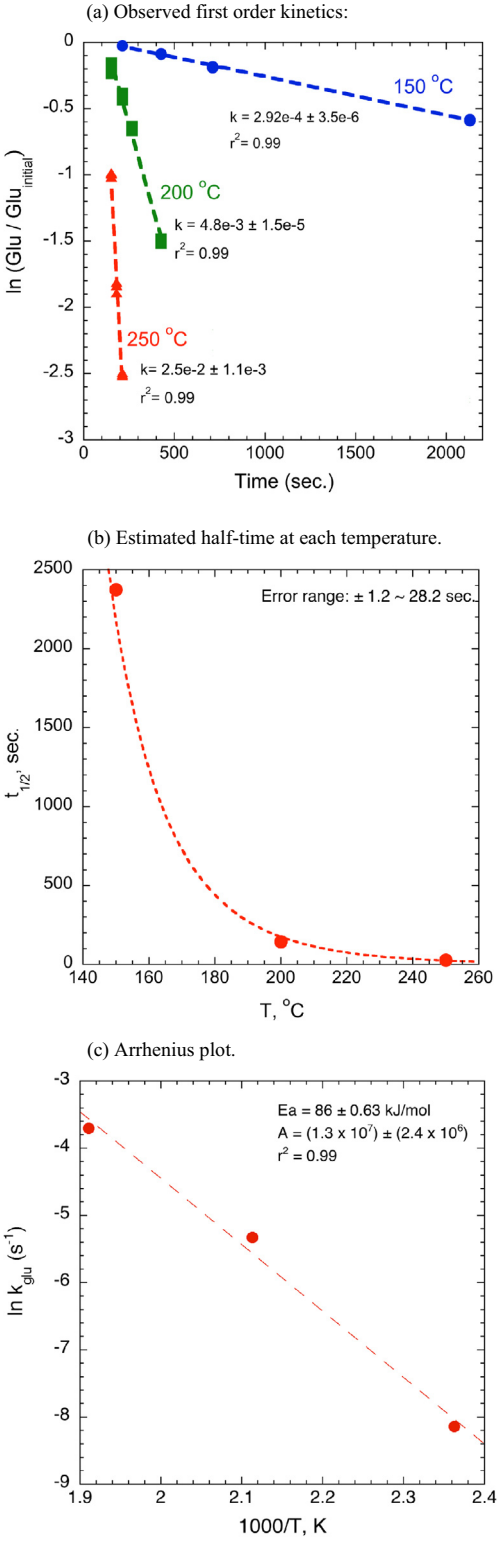

Fig. 4. Kinetic analysis of glutamate conversion to pyroglutamate at high temperature. Data sets with the most analysis points were chosen: for 150 °C, an initial $pH_{25\,°C}$ of 10 with no H_2 added was used; for 200 and 250 °C the data with an initial $pH_{25\,°C}$ of 10 with H_2 were employed.

Table 2
Kinetic data for the conversion of glutamate into pyroglutamate.

T (°C)	k (s^{-1})	$t_{1/2}$ (min)
150	2.9e−4 ± 3.5e−6	40.0
200	4.8e−3 ± 1.5e−5	2.4
250	2.5e−2 ± 1.1e−3	0.5

E_a (apparent activation Energy): 86 ± 0.63 kJ mol^{-1}
A (pre-exponential factor): $1.3 \times 10^7 \pm 2.4 \times 10^6$ s^{-1}

simultaneous with the conversion reaction, glutamate decomposes to products including ammonia, formic acid, $CO_{2(aq)}$, $H_{2(aq)}$, succinic acid, glutaconic acid, and α-hydroxyglutaric acid. Generally, the concentrations of the products increased progressively with reaction time and temperature when H_2 was not added to the solutions (Lee et al., in preparation). In the current study, we observed differences in the abundance of decomposition products as a function of the two initial pH values and again observed the concentration of the decomposition products being strongly dependent on the redox state of the system at all pH conditions (Table 1).

3.2.1. Redox dependence at initial pH = 6

Experimental results corresponding to a $pH_{25\,°C}$ of 6 are depicted in Fig. 5a–g. The most abundant reaction product was ΣCO_2 (equal to the sum of $CO_{2,aq}$, HCO_3^- and CO_3^{2-}) generated progressively with reaction time and temperature. For example, with an initial $pH_{25\,°C}$ of 6 at 200 °C without H_2 added, CO_2 was produced from 0.07 mM up to ~0.2 mM. However, with H_2 set at 13 mM, the CO_2 produced was limited to an approximately constant concentration of about ~0.04 mM (Fig. 5a). At 250 °C and for reducing redox conditions, ΣCO_2 concentrations were also low at about ~0.08 mM (Fig. 5b). Clearly under reducing conditions formation of CO_2 is suppressed. It should be emphasized that these results are consistent with our previous study at higher initial $pH_{25\,°C}$ of 10 (Lee et al., in preparation).

Similar trends were observed for formate (Fig. 5c). At 200 °C with no H_2 added, formate concentrations reached ~8 μM but for H_2-enriched solutions no formate was detected (detection limit ~5 μM). Interestingly, at 250 °C where H_2 was added, the amount of formate approached ~28 μM (Fig. 5d). Clearly, formate production is favored at higher temperatures.

In the case of ammonia production, at 200 °C with no H_2 added, ammonia was formed in considerable amounts, approaching 90 μM, whereas in the presence 13 mM of H_2 less than 10 μM of ammonia was formed. As for the formate discussed above, at 250 °C with the H_2-enriched solution, more ammonia was produced as compared to 200 °C. Although the deamination reaction is not a redox reaction, the overall shift of equilibrium toward the persistence of glutamate in the presence of $H_{2(aq)}$ results in ammonia concentrations dependent on the redox state of the system. Finally, the succinic acid produced shows a strong redox dependency at all temperature conditions (Fig. 5g). At 200 °C and for H_2-enriched solutions ($pH_{25\,°C} = 6$), the succinic acid concentration is significantly lower than the value attained under oxidizing conditions. Overall, these results indicate that there is a consistent redox dependence in the production of decomposition products at an initial $pH_{25\,°C}$ of 6 and 200 °C, as shown by the limited and/or constant value of reaction products when H_2-enriched solutions were used. The absolute abundances of the reaction products are also affected by temperature and by pH (see below). These observations are not unexpected in that previous theoretical calculations have indicated that redox is only one of the major variables inducing the persistence of biomolecules in metastable states (Shock, 1990b, 1992; Shock and Canovas, 2010).

It should be noted that the high concentration of $CO_{2(aq)}$ compared to other reaction products can be explained by the fact that one mol of glutamic acid can ultimately produce up to 5 mol of CO_2 according to

$$C_5H_9NO_4 + 6H_2O = NH_3 + 9H_2O + 5CO_2 \quad (4)$$

Furthermore, one mol of succinic acid can decompose to produce up to 4 mol of CO_2, and one mol of formic acid can decompose to produce an additional mol of CO_2. Indeed, we observe CO_2 ~3 times and ~5 times higher than NH_4^+ for initial $pH_{25\,°C}$ values of 6 and 10, respectively.

3.2.2. Comparison of the effects of different initial pH values

When comparing the types of decomposition products at different pH values observed, we did not see any differences in the species of molecules. However, there were differences in the abundances of each decomposition product detected with varying pH values (Table 1). The diagrams in Fig. 6a–f enable a direct comparison of the different quantities of each decomposition product at initial $pH_{25\,°C}$ values of 6 and 10. At an initial $pH_{25\,°C}$ of 6, the total dissolved CO_2 species produced were approximately 2–3 times lower than that at $pH_{25\,°C}$ of 10 under all redox conditions. In the H_2-free system at 200 °C and for initial $pH_{25\,°C}$ of 10, the $CO_{2(aq)}$ reached ~0.45 mM whereas with initial $pH_{25\,°C}$ of 6, the $CO_{2(aq)}$ produced was limited to ~0.2 mM (Fig. 6a). In the same manner, for H_2-enriched solutions, the total dissolved CO_2 at an initial $pH_{25\,°C}$ of 6 is consistently 2–3 times lower than for an initial $pH_{25\,°C}$ of 10 (Fig. 6b, c).

In the case of the formate at initial $pH_{25\,°C}$ of 6, the concentrations were much lower than for the solutions with an initial $pH_{25\,°C}$ of 10 (Fig. 6d, e). However, at 250 °C, the reverse trend is exhibited, where the formate and ammonia were formed at higher concentrations for an initial $pH_{25\,°C}$ of 6 than for initial $pH_{25\,°C}$ of 10 in the presence of H_2 (Fig. 6f, g). As noted above, the temperature increase from 200 to 250 °C leads to a significant increase in formate and ammonia formation. We speculate that there may be a greater thermodynamic drive at low pH conditions that favors or/and expedites the deamination and decomposition of glutamate.

In effect, the decomposition product analyses show that at an initial $pH_{25\,°C}$ of 6, CO_2 and formate were produced in smaller quantities than with an initial $pH_{25\,°C}$ of 10 at 200 °C. However, at 250 °C with an initial $pH_{25\,°C}$ of 6, formate and ammonia appear to form more readily than at an initial $pH_{25\,°C}$ of 10, as does succinic acid. These results show that in addition to redox, the pH and temperature

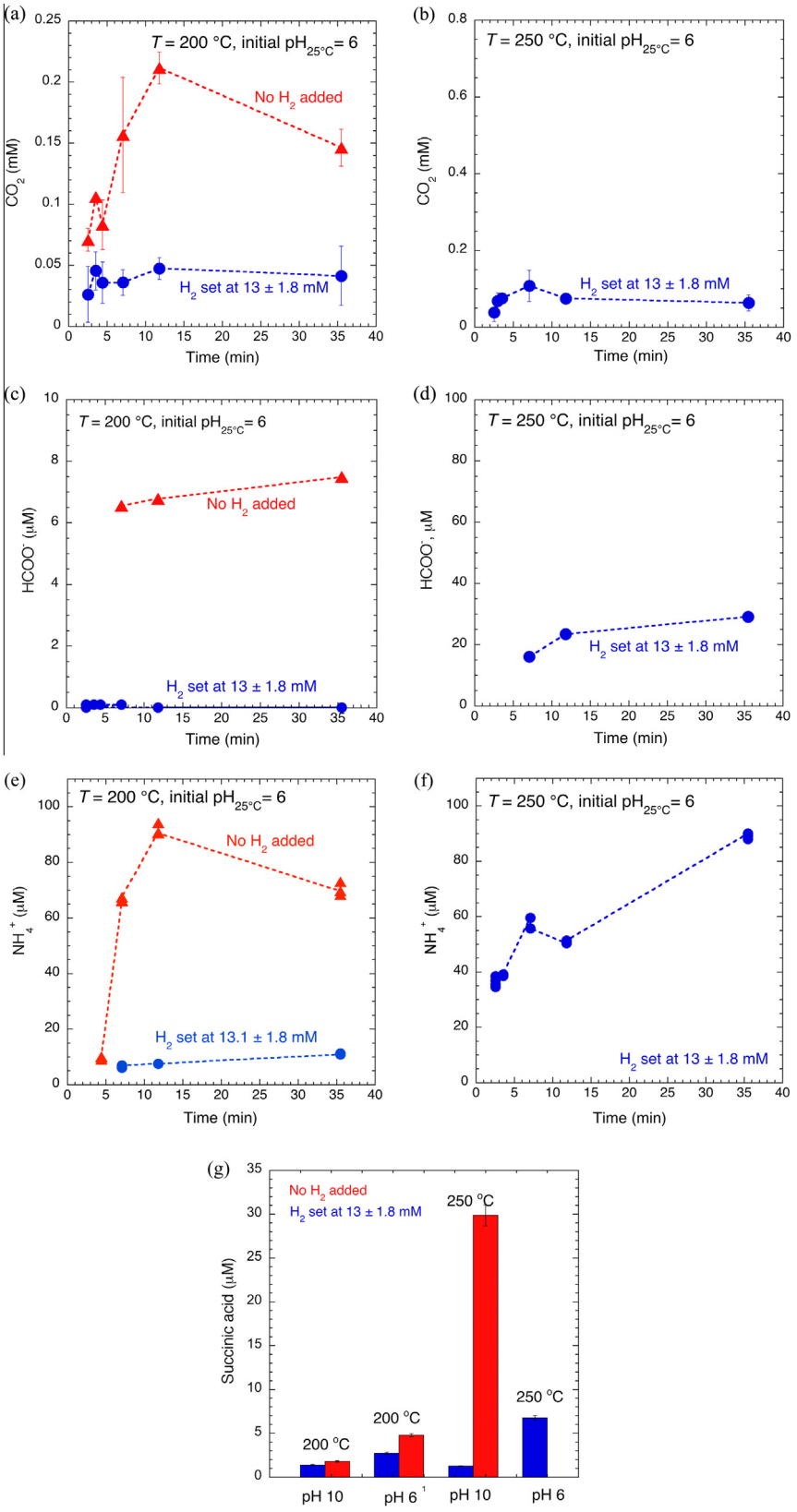

Fig. 5. (a, b) Dissolved CO_2, (c, d) formate, (e, f) ammonium ion (errors bars are within the symbols) and (g) succinic acid produced from the decomposition of glutamate/pyroglutamate at 200 °C and 250 °C with and without the present of dissolved H_2, at initial $pH_{25\,°C} = 6$. Succinic acid concentrations correspond to samples with the longest reaction time.

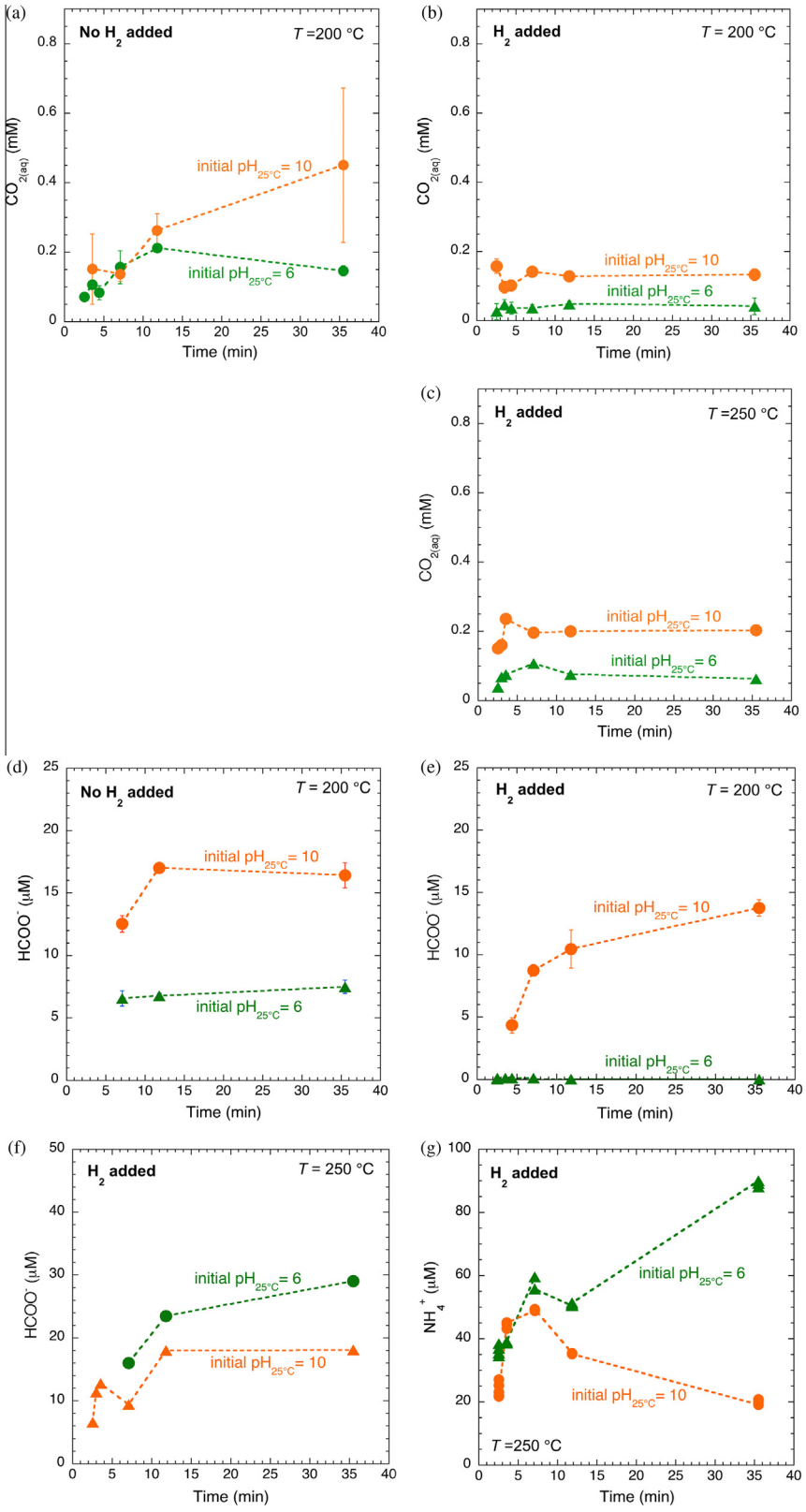

Fig. 6. Comparative plots of decomposition products produced at different initial values of $pH_{25\,°C}$ and temperature. Initial $pH_{25\,°C}$ 10 data are from our another paper (Lee et al., in preparation): (a, b) $CO_{2(aq)}$ produced at 200 °C without and with H_2 added (c) $CO_{2(aq)}$ produced at 250 °C with H_2 added. (d, e) Formate produced at 200 °C without and with H_2 added. (f) Formate produced at 250 °C with H_2 added. (g) Ammonium produced at 250 °C with H_2 added.

are key variables that determine the decomposition process of biomolecules under hydrothermal conditions. Although we do not fully understand the detailed mechanisms of the decomposition process that lead to the different behavior for different pH conditions, it is interesting to observe that the pH in addition to the redox state also results in differences in the amounts of decomposition products. Our results suggest that pH may be another key variable that changes the survivability or stability of biomolecules under hydrothermal conditions. Overall, our results reveal the strong, coherent redox-dependency of glutamate decomposition regardless of pH and temperature demonstrating the critical role of redox state.

3.3. Thermodynamic calculations of *in situ* aqueous speciation

A series of thermodynamic calculations have been conducted to estimate the *in situ* distribution of aqueous species and pH in the experimental hydrothermal solutions. The calculations were performed using the computer program EQ3NR (Wolery, 1992). The equilibrium constants used in the calculations were calculated using SUPCRT92 (Johnson et al., 1992) with revised thermodynamic data from Shock et al. (1997) and Sverjensky et al. (1997) as noted in Table 3. In particular, the thermodynamic properties of aqueous glutamic acid and glutamate given in Table 3 represent a revision based on standard partial molar heat capacities and volumes as functions of temperature from Hakin et al. (1994) and Ziemer and Woolley (2007). Aqueous ionic activity coefficients were calculated using the extended Debye-Hückel equation (Helgeson et al., 1981). Activity coefficients of neutral aqueous species were assumed to be equal to unity. Based on measurements of quenched aqueous species concentrations at each step of the reaction when samples were taken and analyzed, the *in situ* pH and aqueous speciation were calculated.

In the first stage of the calculation, the aqueous speciation of the reactant solutions at 25 °C were assessed. Mass balance, charge balance and mass action expressions were used to calculate the sodium concentrations of the glutamic acid solutions at 25 °C, consistent with the measured pH after addition of NaOH in order to assure charge balance. The resulting sodium concentrations were consistent with the amounts of NaOH added. Subsequently, the results of these calculations were used together with the analytical values of total dissolved glutamate and total dissolved carbonate, aqueous hydrogen (H_2) and ammonia as input constraints. Speciation calculations were then carried out at the experimental temperatures and at 25 °C. In these cases, the *in situ* $pH_{250\,°C}$ was calculated based on mass and charge balance of measured aqueous species and its temperature jump to hydrothermal conditions. The resulting values at the experimental temperatures were taken to represent the *in situ* pH values. The values at 25 °C were taken to represent estimates of the quenched pH values. The latter were measured immediately after reaction using paper pH indicators. The post reaction measured quenched pH values and the estimated quenched pH values are in good agreement, within about ±0.1 pH units (Table 4).

Table 3
Equilibrium constants used in the speciation model.

Reactions	log K values		
	25 °C	200 °C	250 °C
$NaOH = Na^+ + OH^-$	0.20	−0.82	−1.24
$HCOOH = HCOO^- + H^+$	−3.75	−4.45	−4.48
$NH_4OH = NH_4^+ + OH^-$	−4.75	−5.53	−6.05
$OH^- + H^+ = H_2O$	14.00	11.28	11.17
Glutamate + H^+ = Glutamic acid	4.28	5.06	5.57
$CO_{2(aq)} + H_2O = H^+ + HCO_3^-$	−6.35	−7.20	−7.79
$HCO_3^- = H^+ + CO_3^{2-}$	−10.33	−10.47	−10.87

Table 4
pH measurements and estimations.

Conditions	Initial $pH_{25\,°C}$ measured	*In situ* $pH_{250\,°C}$ estimated	Quenched $pH_{25\,°C}$ measured	Quenched $pH_{25\,°C}$ estimated
No H_2 added	10 ± 0.01	7.2 ± 0.03	9.6 ± 0.05	9.7 ± 0.03
H_2 added	10 ± 0.01	7.3 ± 0.03	9.9 ± 0.05	10 ± 0.03
H_2 added	6 ± 0.01	6.7 ± 0.03	5.7 ± 0.05	5.8 ± 0.03

The estimated *in situ* pH values are plotted in Fig. 7a and b at 250 °C. For the case of an initial $pH_{25\,°C}$ 10 with H_2 added, the calculations gave *in situ* pH values of about ~7.3, much less than 10, and this pH did not change significantly over the reaction time when H_2 was present (Fig. 7a). This result is partly attributable to the fact that rather low concentrations of decomposition products were detected when H_2 was imposed on the system. When H_2 was not present there was a very slight continuous decrease of the pH to about 7.2 (Fig. 7a), which may correspond to the progressively increasing concentrations of decomposition products noted above for these conditions. In contrast, it can be seen in Fig. 7b that in the case of a solution with an initial $pH_{25\,°C}$ of 6 with H_2 added, the *in situ* pH was estimated to be about 6.8, which is higher than the initial $pH_{25\,°C}$. These differences arise from the initial pH values (at 25 °C) in the experiments. Before discussing this we first discuss the speciation results for the other species shown in Fig. 7c–f.

The main result of the speciation calculations for the product species is that the dominant species under all conditions are $CO_{2(aq)}$, $HCOO^-$, and $NH_{3(aq)}$. Fig. 7c shows that at 250 °C with an initial $pH_{25\,°C}$ of 10 where no H_2 was added, there is a continuous increase of $CO_{2(aq)}$, and HCO_3^- and a small increase in $HCOO^-$. In contrast, under the same condition but with H_2 added (Fig. 7d), there are lower and approximately constant values of $CO_{2(aq)}$, bicarbonate and formate. Similarly, at 250 °C with an initial $pH_{25\,°C}$ of 6 and H_2-enriched solutions there are even lower, but still approximately constant, values of all the aqueous species throughout the reaction time compared with an initial $pH_{25\,°C}$ of 10 (Fig. 7e). However, the major difference between the initial pH values of 6 and 10 in the speciation results can be seen in Fig. 7f for the aqueous ammonia species. For the initial $pH_{25\,°C}$ of 6, $NH_{3(aq)}$ is continuously created through the reaction sequence. However for the initial $pH_{25\,°C}$ of 10, only small amounts of $NH_{3(aq)}$ are created. The difference between Fig. 7d and e lies mainly in the different amounts of $CO_{2(aq)}$ produced.

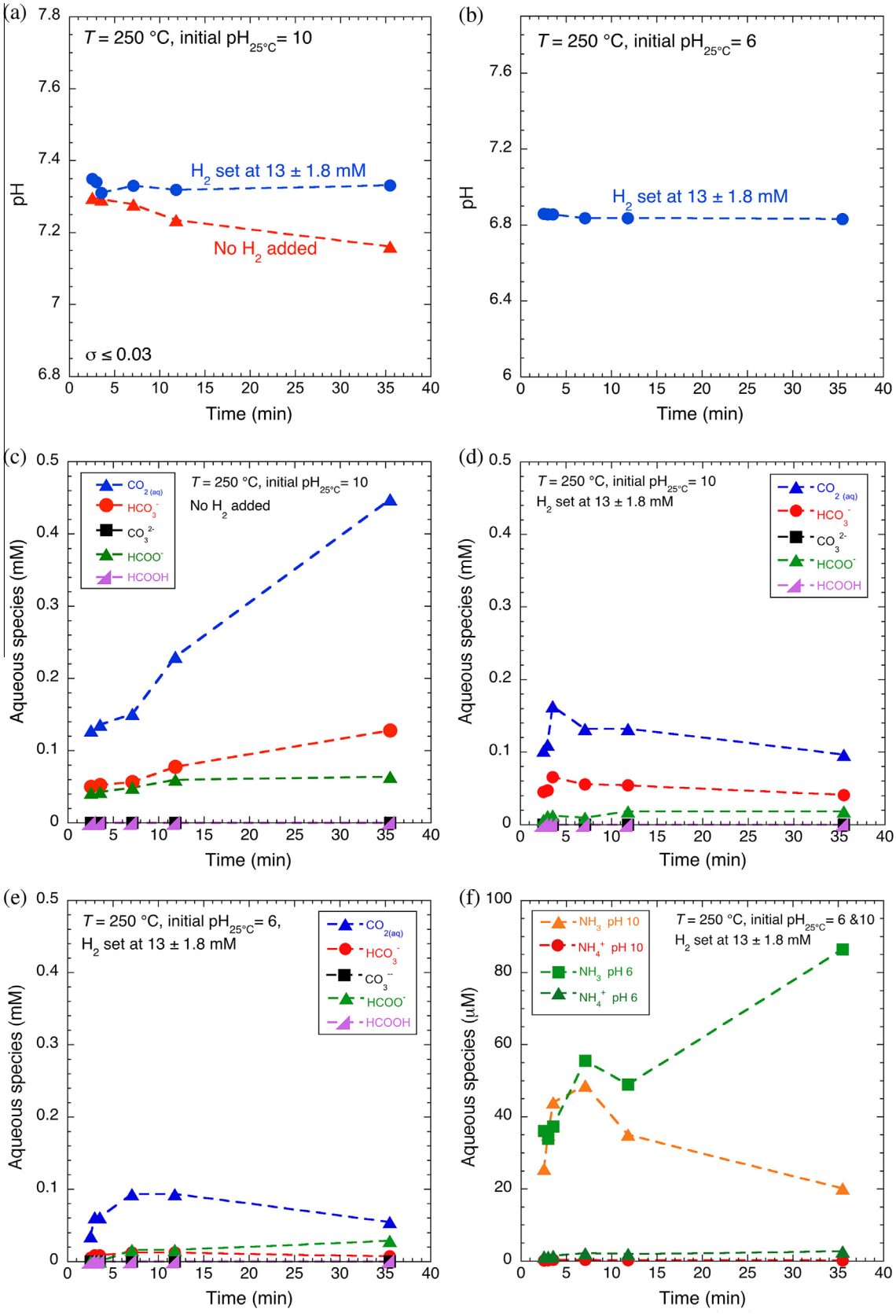

Fig. 7. Calculated (a, b) *in situ* pH and (c–e) aqueous speciation at different conditions.

Overall, the speciation calculations referring to 250 °C summarized in Fig. 7a–f indicate fluids in which the dominant species present at elevated temperatures are glutamate (pyroglutamate), Na^+, and OH^-. The fluids are alkaline regardless of the initial starting pH because neutral pH at this temperature is 5.6. The initial pH values of 6 and 10 at 25 °C change to their high-temperature values of about 6.8 and 7.3, respectively at 250 °C when H_2 is present for different reasons. For the solutions with initial pH of 6 at 25 °C, the H^+ and OH^- are both present in very low concentrations. At high temperature, when the water dissociates, both H^+ and OH^- are affected, without much change on pH. Consequently, proton reactions involving other species are important. By far the most abundant species is glutamate which associates with protons more strongly at 250 °C. This consumption of protons by glutamate to produce some H-glutamate increases the pH towards 6.8 at 250 °C. The production of the neutral species $CO_{2(aq)}$ in place of glutamate also results in a net consumption of H^+. However, for the solutions with initial $pH_{25\,°C}$ of 10 at 25 °C, the OH^- is extremely abundant relative to the H^+. In this case, the high temperature dissociation of water increases the H^+ abundance dramatically, without increasing the already abundant OH^- significantly. Consequently, these solutions at high temperature show a strong decrease of the pH from 10 to about 7.3 at 250 °C.

The detailed calculated distribution of carbonate and formate species with known concentrations of $H_{2(aq)}$ under hydrothermal conditions enables further examination of possible metastable equilibria amongst these species (McCollom and Seewald, 2003b). For example, the equilibrium between HCO_3^- and $HCOO^-$ can be expressed by

$$HCOO^- + H_2O = HCO_3^- + H_{2,aq} \quad (5)$$

The corresponding mass action equation can be written as

$$\log \frac{a_{HCO_3^-}}{a_{HCOO^-}} = \log K + \log a_{H_2} \quad (6)$$

where the activity coefficient of aqueous H_2 is assumed to be equal to unity for highly diluted aqueous electrolyte solutions. According to Eq. (6), at a given temperature and pressure, the ratio of the bicarbonate/formate species should be determined by the H_2 concentration. We used the calculated speciation reported above to compute the logarithmic ratios of HCO_3^- and $HCOO^-$ in the experimental solutions and compared them with the theoretically calculated ratios that correspond to the measured $H_{2(aq)}$ concentrations. The results are illustrated in Fig. 8.

Firstly, when no H_2 was added, the system is far from equilibrium and this state does not change significantly during the reaction times investigated (Fig. 8a). From this it can be inferred that the reaction products are being formed at a much faster rate than the time required for the bicarbonate/formate system to equilibrate. On the other hand, with 13 ± 1.8 mM of dissolved H_2 in the solution, at 250 °C with an initial $pH_{25\,°C}$ of 10, the system approaches the equilibrium value within ~15 min. Similarly, fluids with an initial $pH_{25\,°C}$ of 6 with H_2 added also approach equilibrium within the given reaction time. The equilibration timescale of about 35 min observed in our experiments is a dramatic contrast to the much longer equilibration times of many tens of hours in earlier studies. For example, McCollom and Seewald (2003a) studied formic acid decomposition at 250 °C with no minerals present or any H_2 added. Under these circumstances metastable equilibrium was approached in about 69 h. We wish to note that their reaction vessel was made of the same type of oxidized Ti-alloy as ours, which rules out a difference in catalysis by the containers. We can infer from this comparison that our H_2-free experiments (Fig. 8a) may have been much too short to reach equilibrium in the C–O–H system or, as indicated above, the rates of glutamate decomposition were too fast for the C–O–H metastable equilibrium to be reached. In contrast, the rapid equilibration observed in the H_2-added experiments remains unexplained (Fig. 8b, c).

3.4. Proposed reaction mechanisms and metastable equilibria

The products of the decomposition of glutamate, including total dissolved CO_2, HCOOH, succinic acid, hydroxyglutaric acid and glutaconic acid, can be related to the following proposed reaction mechanisms as shown in Fig. 9a–c. First the measured decomposition products are most abundant when no H_2 was added. We consider this case in Fig. 9a, which corresponds most closely to the results of previous decomposition studies of amino acids and other organics where experiments were conducted without any redox control (Bada and Miller, 1970; Andersson and Holm, 2000; Bada et al., 1995; Cox and Seward, 2007a,b; Lemke et al., 2009; McCollom, 2013). It can be seen in Fig. 9a that glutamate (in equilibrium with pyroglutamate) is expected to deaminate, forming glutaconic acid. This reaction is expected to be reversible under hydrothermal conditions by analogy with studies of aspartic acid (Bada and Miller, 1968, 1970). Subsequently glutaconic acid may dehydrate, forming hydroxyglutaric acid in the α-form. Again this reaction is expected to be reversible as has been recently demonstrated in analogous studies of aromatic ketones, alcohols and related hydrocarbons (Yang et al., 2012). This step is followed by α-hydroxyglutaric acid undergoing a dehydrogenation reaction, forming α-ketoglutaric acid – a critical step in the sequence that is also expected to be reversible (Seewald, 1994, 2001; Yang et al., 2012). However, the α-ketoglutaric acid is expected to decarboxylate irreversibly to succinic acid and formic acid. Under these circumstances, α-hydroxyglutaric acid is continuously lost resulting in an accumulation of reaction products as a function of time and temperature.

It should be emphasized that in this reaction sequence the only redox-dependent step is the dehydrogenation of α-hydroxyglutaric acid to α-ketoglutaric acid:

$$\text{α-hydroxyglutaric acid} = \text{α-ketoglutaric acid} + H_{2,aq} \quad (7)$$

Based on the corresponding mass action expression, and again assuming a unit activity coefficient for aqueous H_2, we can write

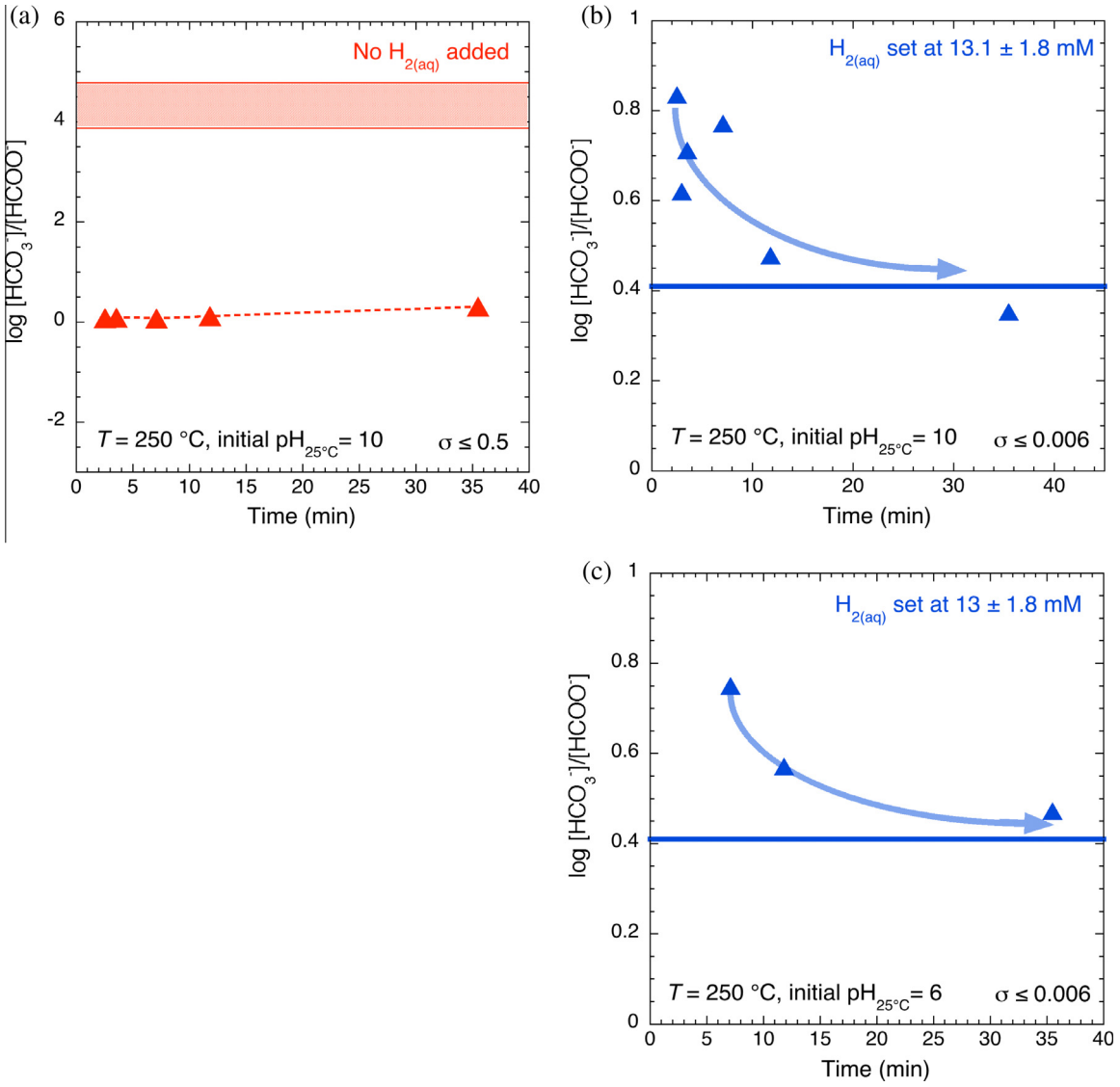

Fig. 8. Formate-CO_2 speciation in the hydrothermal experiments compared with hypothetical conditions of metastable equilibria. The symbols represent the speciated experimental hydrothermal fluids and the solid lines or bands represent calculated theoretical equilibrium state: (a) At 250 °C, initial $pH_{25\,°C} = 10$ and no H_2 added, the system is far from the equilibrium state. (b) At 250 °C, initial $pH_{25\,°C} = 10$ and for $pH_{25\,°C} = 6$ (c) with H_2 added, dissolved species approach equilibrium.

$$\log \frac{a_{\alpha\text{-ketoglutaric}}}{a_{\alpha\text{-OH-glutaric}}} = \log K - \log m_{H_{2,aq}} \quad (8)$$

from which it is apparent that low values of dissolved $H_{2(aq)}$ will favor higher amounts of the ketoglutaric acid relative to hydroxyglutaric acid. In experiments without added $H_{2(aq)}$, only very small amounts of $H_{2(aq)}$ actually formed in the system (<5 μM), which apparently strongly favored the formation of ketoglutaric acid, which decomposed irreversibly to formic and succinic acids, which in turn resulted in elevated dissolved $CO_{2(aq)}$ concentrations.

Second, consider the case in Fig. 9b corresponding to the situation where the redox state of the system was controlled by imposing 13 ± 1.8 mM dissolved $H_{2(aq)}$. Under these circumstances, the reducing conditions correspond to about 10,000 times more $H_{2(aq)}$ in Eq. (8) than when no H_2 was added to the solutions. This lowers the amount of ketoglutaric acid relative to hydroxyglutaric acid by a factor of 10,000, effectively inhibiting the redox reaction from α-hydroxyglutaric acid to α-ketoglutaric acid. In turn, this is expected to shift all the reversible equilibria depicted in Fig. 9b back towards favoring the persistence of glutamate, which explains why the $H_{2(aq)}$-enriched solutions resulted in much lower and generally essentially constant amounts of reaction products.

An alternate reaction mechanism that might be expected is depicted in Fig. 9c. In this scenario, the redox-sensitive reaction occurs as the first step through the formation of an imine. The 2-imminoglutaric acid subsequently would be expected to dehydrate, forming 2-hydroxyglutamic acid followed by a deamination reaction to α-ketoglutaric acid. After that, the reaction path would be the same as depicted in Fig. 9a, according to which the α-ketoglutaric acid

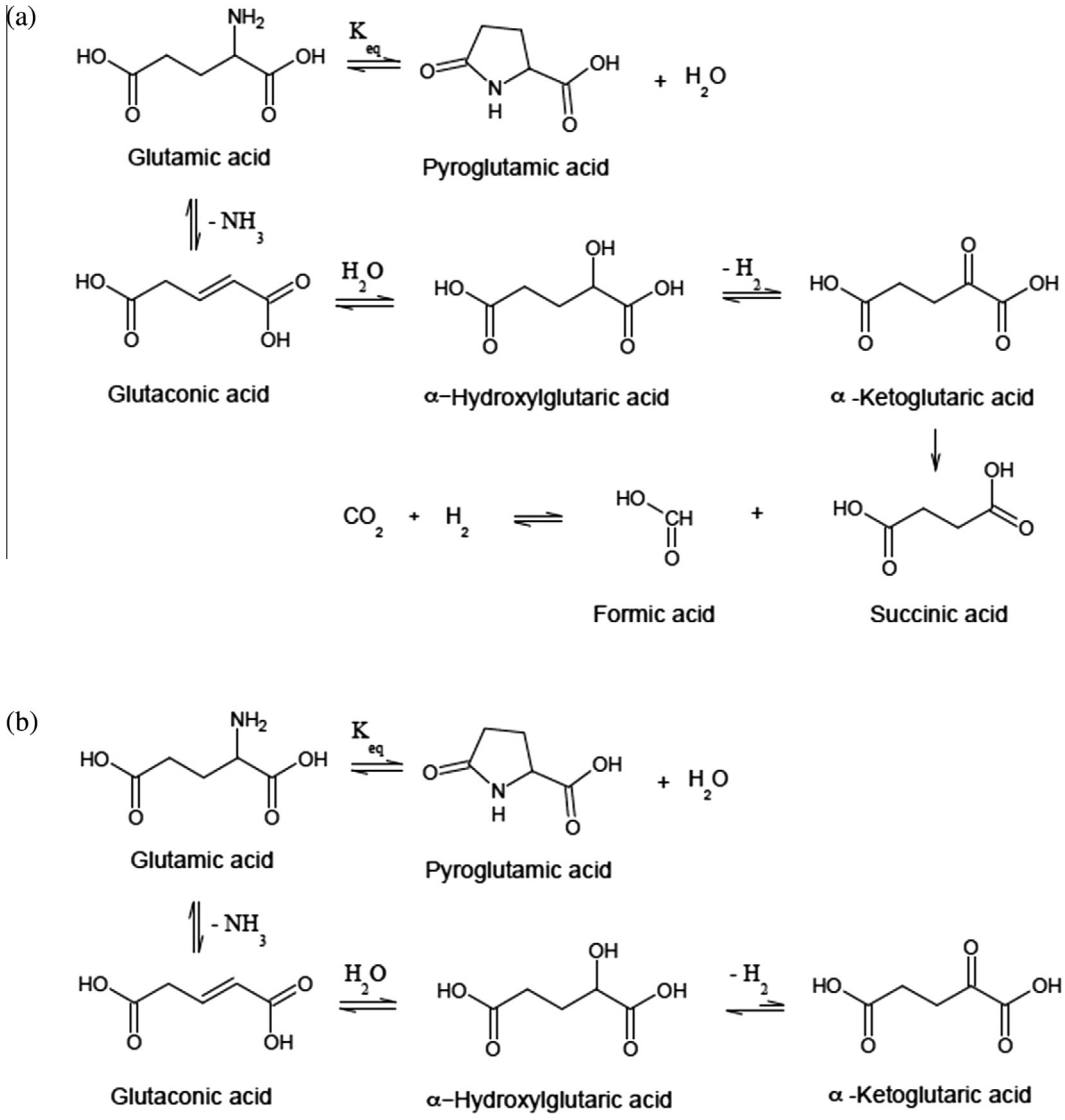

Fig. 9. Proposed reaction mechanisms for glutamate under hydrothermal conditions (a) Reaction mechanism where no H_2 was added. The reaction proceeds to final product of CO_2 and H_2 without any inhibition. Accumulative reaction products were detected. (b) Reaction mechanism for H_2 enriched solutions. Due to the high concentration of H_2, the reaction is inhibited at redox reaction from α-hydroxyglutaric acid to α-Ketoglutaric acid. Clearly limited amounts of decomposition products were detected under these conditions. (c) Extended reaction mechanism where the glutamate directly goes through redox reaction forming 2-iminoglutaric acid simultaneous to deamination reaction. Although we did not detect this molecule, this path way is also possible.

decarboxylates to succinic and formic acids. We do not consider this to be as significant a pathway for our system as the ones depicted in Fig. 9a and b, because we did not detect 2-hydroxyglutamic acid.

Overall, our experimental results are consistent with the hypothesis of metastable equilibria between the reaction products containing five carbon atoms depicted in Fig. 9a and b, i.e. between glutamic (and pyroglutamic), glutaconic, hydroxyglutaric and ketoglutaric acids. This result implies an overall metastable equilibrium between glutamic and ketoglutaric acids. Assuming that the main species of these two acids in the hydrothermal experiments are glutamate and α-ketoglutarate, the equilibrium between these species can be written

$$\text{Glutamate}^- + H_2O = \alpha\text{-ketoglutarate}^- + H_{2,aq} + NH_{3,aq} \quad (9)$$

and the corresponding mass action expression can be expressed by

$$\log a_{H_{2,aq}} = \log a_{NH_{3,aq}} + \log K - \log \frac{m_{\alpha\text{-ketoglutarate}}}{m_{\text{glutamate}}} \quad (10)$$

The equilibrium constant in Eq. (10) has been evaluated using the thermodynamic data and estimation schemes for α-ketoglutarate$^-$ from a recent study (Dalla-Betta and Schulte, 2009) and data for the other species in Eq. (10) from the sources discussed above (Table 1). It should be

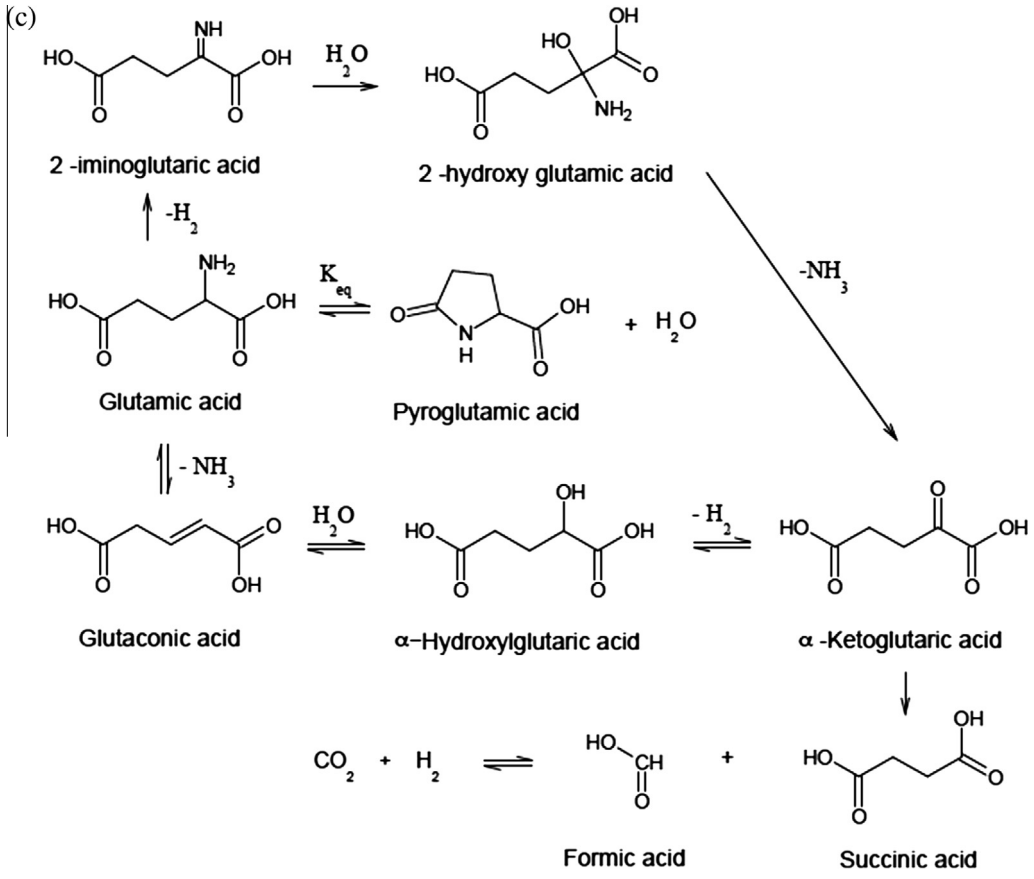

Fig 9. *(continued)*

emphasized that some uncertainty is associated with the thermodynamic characterization of α-ketoglutarate at elevated temperatures. The free energy of formation at ambient conditions was taken from the detailed investigation of a network of biochemically relevant aqueous organic species (Miller and Smith-Magowan, 1990). More recent studies have been carried out on a less general network of reactions (Alberty, 2005). However, the temperature dependence of the free energy of the α-ketoglutarate also relies on estimations of the standard partial molal entropy and heat capacity, which may contribute uncertainties of the order of at least ±0.3 units in the calculated log$K$ values at the temperatures of our experiments.

The boundaries in Fig. 10a and b represent calculations based on Eq. (10) at 200 and 250 °C, respectively. The lines depicted on each diagram correspond to concentration ratios of glutamate to α-ketoglutarate from 0.1 to 10. The symbols on the figures represent the specific conditions for our experiments discussed above. In comparing the relative positions of the lines in Fig. 10a and b, it can be seen that lower temperature enhances the predominance field of glutamate relative to α-ketoglutarate. At both temperatures, our experiments without $H_{2(aq)}$ added are clearly in the field of α-ketoglutarate. However, the H_2-bearing experiments are either close to or in the predominance field of glutamate, in that they lie close to or even on the glutamate side of the speciation boundaries. Although the exact ratios of glutamate relative to α-ketoglutarate in the experiments are not known, and probably vary as a function of reaction progress, these results provide strong theoretical support for the metastable equilibria depicted in Fig. 9a and b above.

Diagrams such as those shown in Fig. 9a and b could be used in the planning of future experimental studies involving the hydrothermal conditions under which amino acids and other biomolecules might show geochemically important equilibrium relationships. More specifically, in seeking to understand the precise mechanisms of hydrothermal organic reactions, such diagrams will facilitate delineating the conditions under which certain reaction intermediates might be most easily detected and quantified. Until this study, such approaches have been limited to systems involving molecules with only one or two carbon atoms (e.g. Seewald, 1994; Seewald et al., 2006). It appears now that much larger organic molecules may also participate in metastable hydrothermal equilibria (c.f. Yang et al., 2012).

4. CONCLUDING REMARKS

In the present study, we have reported on the effect of redox state on the stability of glutamic acid controlled by 13 mM dissolved $H_{2(aq)}$ at temperatures of 150, 200 and 250 °C and initial pH values of 6 and 10 in a flow-through

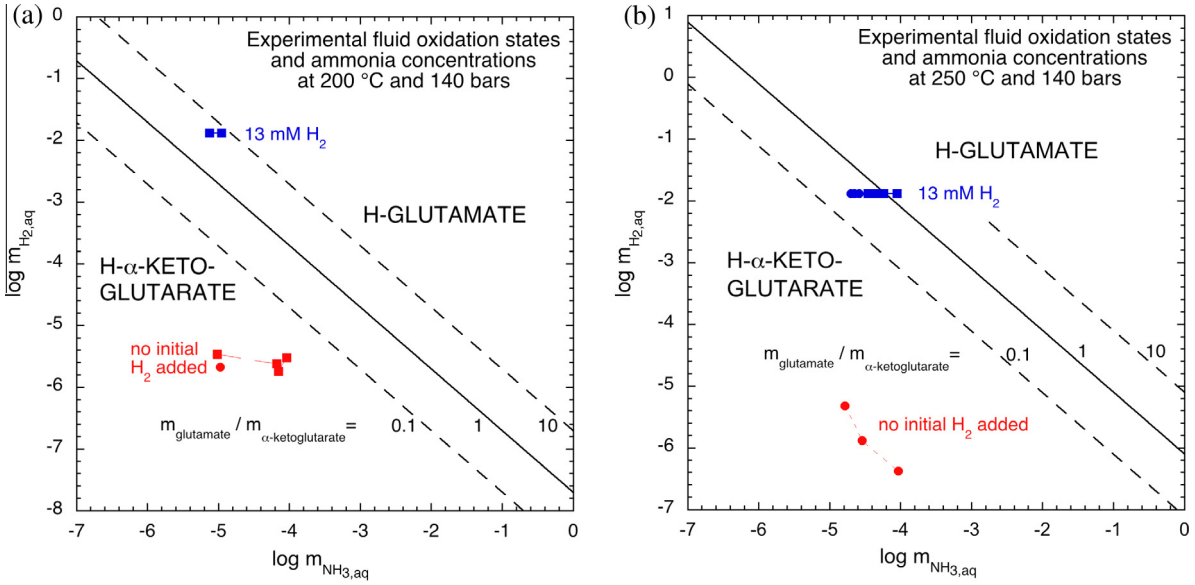

Fig. 10. Aqueous activity diagrams for glutamate stability relative to α-ketoglutarate plotted in terms of the log molality of ammonia versus log molality of aqueous H_2. The solid circle symbols represent experimental solutions with an initial $pH_{25\,°C}$ of 10 and the solid square symbols represent experimental solutions with initial $pH_{25\,°C}$ of 6. The lines depicted on each diagram correspond to concentration ratios of glutamate to α-ketoglutarate assumed equal to a range of values from 0.1 to 10.0 at 200 °C (a) and at 250 °C (b). For both initial pH conditions with no H_2 added, the experimental solutions are located within the α-ketoglutarate predominance field moving towards higher concentrations of ammonia as the reaction progress. However, the experimental solutions with 13 mM H_2 added lie in the glutamate stability field or close to the boundary. This result is consistent with the experimentally observed effect of added H_2 suppressing the decomposition of glutamate.

hydrothermal reactor with reaction times ranging from 3 to 36 min. We combined experimental measurements with theoretical calculations to model the *in situ* aqueous speciation and pH values, and to describe the conditions of metastable equilibria. Based on our measurements and calculations described above, the following conclusions can be drawn:

(1) As previously observed for glutamate under hydrothermal conditions, the main reaction that takes place involves the cyclization of glutamate to pyroglutamate through a simple dehydration reaction.
(2) Decomposition products measured quantitatively include total dissolved succinate, formate, carbon dioxide and ammonia. Decomposition products detected qualitatively using GC–MS include glutaconic acid and α-hydroxyglutaric acid.
(3) The amounts of succinate, formate, carbon dioxide and ammonia depend on the temperature, the pH and particularly the redox state of the fluid. Without added $H_{2(aq)}$, glutamate decomposes, ultimately to CO_2, formate and micromolar quantities of $H_{2(aq)}$. Model speciation calculations indicate these species are not in metastable equilibrium on the short timescale of our experiments. However, for $H_{2(aq)}$-enriched solutions, the amounts of decomposition products are suppressed at all the conditions (T, pH) investigated. The very minor amounts of CO_2 and formate (and the 13 ± 1.8 mM $H_{2(aq)}$) are expected to approach a metastable equilibrium according to the reaction

$$HCOO^- + H_2O = HCO_3^- + H_2$$

(4) It is proposed that glutamic acid first deaminates to glutaconic acid, which dehydrates to α-hydroxyglutaric acid followed by dehydrogenation to ketoglutaric acid. These three steps are suggested to correspond to reversible equilibria by analogy with recent studies of aromatic hydrocarbons (Yang et al., 2012) and other studies of hydrocarbons and related compounds (Seewald, 2001).
(5) The redox-sensitive decomposition of glutamate is suggested to be controlled by the reaction of α-hydroxyglutarate to α-ketoglutarate:

$$\text{α-hydroxyglutaric acid} = \text{α-ketoglutaric acid} + H_{2(aq)} \quad (11)$$

This reaction shows that the formation of α-ketoglutaric acid is effectively inhibited at elevated $H_{2(aq)}$ concentrations, which causes a dramatic decrease in the amounts of all the decomposition products of α-ketoglutaric acid, such as succinic and formic acids and $CO_{2(aq)}$.
(6) Theoretical thermodynamic calculations indicate that the experimental results with and without $H_{2(aq)}$ added are consistent with an overall metastable equilibrium between glutamate and α-ketoglutarate according to the reaction

$$\text{Glutamate}^- + H_2O = \text{α-ketoglutarate}^- + H_{2(aq)} + NH_{3(aq)} \quad (12)$$

High levels of dissolved $H_{2(aq)}$ in our experiments cause a dramatic decrease in the amounts of decomposition products, including $NH_{3(aq)}$. However, this is also a function of temperature, so that results at 200 and 250 °C differ in some details.

(7) Our findings establish that redox state is as important a variable as temperature and pH in affecting the stability of amino acids under hydrothermal conditions. It is suggested that when natural hydrothermal fluids contain enough dissolved $H_{2(aq)}$, the stability of amino acids may be enhanced, at least on short timescales. In turn, this result suggests that reducing hydrothermal environments may have been favorable for assembling the building blocks of biomolecules in the origin of life (Shock and Canovas, 2010).

(8) Our findings also have implications for present-day life in mid-ocean ridge hydrothermal systems. The mixing between hydrothermal fluids and the cold oxygenated seawater induces redox gradients that constrain the series of chemolithoautotrophic metabolic processes that support unique ecosystems in deep-sea microbial communities (Edwards et al., 2005). Recently it has been shown that when $H_{2(aq)}$ functions as an electron donor, it could support anaerobic chemosynthetic microorganisms growing over a wide range of temperatures, including the symbiotic bacteria in hydrothermal vent mussels, tubeworms and shrimp (Petersen et al., 2011; Wankel et al., 2011). If amino acid stability is enhanced in such systems by the presence of dissolved $H_{2(aq)}$, then the reduced nature of the fluids might play a role in supporting heterotrophic microbial communities. These findings throw new light on the role of hydrogen in microbial metabolism, thus expanding our concepts of the diversity of the subsurface biosphere and symbiotic life near hydrothermal vent environments.

ACKNOWLEDGMENTS

The authors greatly appreciate discussions with and assistance in the laboratory from M.L. Fogel, I. Pérez-Rodríguez, C.F. Estrada, K. Klochko and S. Ohara. In addition, N. Lee acknowledges inspirational advice from Bjørn Mysen in initiating this study. N. Lee and D.A. Sverjensky greatly appreciate the support of R.J. Hemley during their stay as visiting researchers at the Geophysical Laboratory. This research was conducted with support from the NSF OCE-0928443 (D.F.), NSF OCE-1038114 (D.F.), NSF EAR-1023865 (D.A.S.), DOE DE-FG02-96ER-14616 (D.A.S.), NSF EAR-1023889 (R.M.H.), NASA Astrobiology Institute, and the Carnegie Institution of Washington.

REFERENCES

Alberty R. A. (2005) Calculation of thermodynamic properties of species of biochemical reactants using the inverse Legendre transform. *J. Phys. Chem. B* **109**, 9132–9139.

Amend J. P. and Shock E. L. (1998) Energetics of amino acid synthesis in hydrothermal ecosystems. *Science* **281**, 1659–1662.

Andersson E. and Holm N. G. (2000) The stability of some selected amino acids under attempted redox constrained hydrothermal conditions. *Origins Life Evol. Biosph.* **30**, 9–23.

Bada J. L. and Miller S. L. (1968) Ammonium ion concentration in the primitive ocean. *Science* **159**, 423–425.

Bada J. L. and Miller S. L. (1970) Kinetics and mechanism of the reversible nonenzymic deamination of aspartic acid. *J. Am. Chem. Soc.* **92**, 2774–2782.

Bada J. L., Miller S. L. and Zhao M. X. (1995) The stability of amino acids at submarine hydrothermal vent temepratures. *Origins Life Evol. Biosph.* **25**, 111–118.

Bernhardt G., Lüdemann H.-D., Jaenicke R., König H. and Stetter K. O. (1984) Biomolecules are unstable under "black smoker" conditions. *Naturwissenschaften* **71**, 583–586.

Clarke A. P., Jandik P., Rocklin R. D., Liu Y. and Avdalovic N. (1999) An integrated amperometry waveform for the direct, sensitive detection of amino acids and amino sugars following anion-exchange chromatography. *Anal. Chem.* **71**, 2774–2781.

Cleaves D. W. (1950) An interpretation of the kinetics of glutamic acid lactam formation. *J. Biol. Chem* **163**, 163–165.

Corliss J. B. B. J. A. and Hoffman S. E. (1981) An hypothesis concerning the relationship between submarine hot springs and the origin of life on Earth. *Oceanol. Acta* **4**, 59–69.

Corliss J. B., Dymond J., Gordon L. I., Edmond J. M., Herzen R. P., Ballard R. D., Green K., Williams D., Bainbridge A., Crane K. and Andel T. H. (1979) Submarine thermal springs on the Galapagos Rift. *Science* **203**, 1073–1083.

Cox J. S. and Seward T. M. (2007a) The hydrothermal reaction kinetics of aspartic acid. *Geochim. Cosmochim. Acta* **71**, 797–820.

Cox J. S. and Seward T. M. (2007b) The reaction kinetics of alanine and glycine under hydrothermal conditions. *Geochim. Cosmochim. Acta* **71**, 2264–2284.

Cruse A. M. and Seewald J. S. (2010) Low-molecular weight hydrocarbons in vent fluids from the Main Endeavour Field, northern Juan de Fuca Ridge. *Geochim. Cosmochim. Acta* **74**, 6126–6140.

Dalla-Betta and Schulte M. D. (2009) Calculation of the aqueous thermodynamic properties of citric acid cycle intermediates and precursors and the estimation of high temperature and pressure equation of state parameters *Int. J. Mol. Sci.* **10**, 2809–2837.

Edwards K. J., Bach W. and McCollom T. M. (2005) Geomicrobiology in oceanography: microbe-mineral interactions at and below the seafloor. *Trends Microbiol.* **13**, 449–456.

Ferris J. (1992) Chemical markers of prebiotic chemistry in hydrothermal systems. *Origins Life Evol. Biosph.* **22**, 109–134.

Foustoukos D. I. and Seyfried W. E. (2004) Hydrocarbons in hydrothermal vent fluids: the role of chromium-bearing catalysts. *Science* **304**, 1002–1005.

Foustoukos D. I., Savov I. P. and Janecky D. R. (2008) Chemical and isotopic constraints on water/rock interactions at the Lost City hydrothermal field, 30°N Mid-Atlantic Ridge. *Geochim. Cosmochim. Acta* **72**, 5457–5474.

Foustoukos D. I., Houghton J. L., Seyfried W. E., Sievert S. M. and Cody G. D. (2011) Kinetics of H2–O2–H2O redox equilibria and formation of metastable H2O2 under low temperature hydrothermal conditions. *Geochim. Cosmochim. Acta* **75**, 1594–1607.

Hakin A. W., Duke M. M., Klassen S. A., McKay R. M. and Preuss K. E. (1994) Apparent molar heat capacities and volumes of some aqueous solutions of aliphatic amino acids at 288.15, 298.15, 313.15, and 328.15 K. *Can. J. Chem.* **72**, 362–368.

Helgeson H. C., Kirkham D. H. and Flowers G. C. (1981) Theoretical prediction of the thermodynamic behavior of aqueous-electrolytes at high-pressures and temperatures. IV. Calculation of activity-coefficients, osmotic coefficients, and apparent molal and standard and relative partial molal properties to 600-degrees-C and 5 Kb. *Am. J. Sci.* **281**, 1249–1516.

Helgeson H. C., Knox A. M., Owens C. E. and Shock E. L. (1993) Petroleum, oil field waters, and authigenic mineral assemblages: are they in metastable equilibrium in hydrocarbon reservoirs? *Geochim. Cosmochim. Acta* **57**, 3295–3339.

Hennet R. J. C., Holm N. G. and Engel M. H. (1992) Abiotic synthesis of amino acids under hydrothermal conditions and the origin of life: A perpetual phenomenon? *Naturwissenschaften* **79**, 361–365.

Holm N. G. and Charlou J. L. (2001) Initial indications of abiotic formation of hydrocarbon in the Rainbow ultramafic hydrothermal systen, Mid-Atlanctic Ridge. *Earth Planet. Sci. Lett.* **191**, 1–8.

Huber C. and Wächtershäuser G. (1998) Peptides by activation of amino acids with CO on (Ni, Fe)S surfaces: implications for the origin of life. *Science* **281**, 670–672.

Johnson J. W., Oelkers E. and Helgeson H. C. (1992) SUPCRT92: a software package for calculating the standard molal thermodynamic properties of minerals, gases, aqueous species and reactions from 1 to 5000 bar and 0 to 1000 C. *Comput. Geosci.* **18**, 899–947.

Kelley D. S., Karson J. A., Fruh-Green G. L., Yoerger D. R., Shank T. M., Butterfield D. A., Hayes J. M., Schrenk M. O., Olson E. J., Proskurowski G., Jakuba M., Bradley A., Larson B., Ludwig K., Glickson D., Buckman K., Bradley A. S., Brazelton W. J., Roe K., Elend M. J., Delacour A., Bernasconi S. M., Lilley M. D., Baross J. A., Summons R. T. and Sylva S. P. (2005) A serpentinite-hosted ecosystem: the lost city hydrothermal field. *Science* **307**, 1428–1434.

Konn C., Charlou J. L., Donval J. P., Holm N. G., Dehairs F. and Bouillon S. (2009) Hydrocarbons and oxidized organic compounds in hydrothermal fluids from Rainbow and Lost City ultramafic-hosted vents. *Chem. Geol.* **258**, 299–314.

Lee N., Foustoukos D. I., Sverjensky D. A., Hazen R. M. and Cody G. D. (in preparation) Hydrogen enhances the stability of amino acids in hydrothermal environments.

Lemke K. H., Rosenbauer R. J. and Bird D. K. (2009) Peptide synthesis in early earth hydrothermal systems. *Astrobiology* **9**, 141–146.

Manning C. E., Shock E. L. and Sverjensky D. A. (2013) The chemistry of carbon aqueous fluids at crustal and upper-mantle conditions: experimental and theoretical constraints. *Rev. Mineral. Geochem.* **75**, 109–148.

McCollom T. M. (2013) The influence of minerals on decomposition of the n-alkyl-α-amino acid norvaline under hydrothermal conditions. *Geochim. Cosmochim. Acta* **104**, 330–357.

McCollom T. M. and Seewald J. S. (2003a) Experimental constraints on the hydrothermal reactivity of organic acids and acid anions: I. Formic acid and formate. *Geochim. Cosmochim. Acta* **67**, 3625–3644.

McCollom T. M. and Seewald J. S. (2003b) Experimental study of the hydrothermal reactivity of organic acids and acid anions: II. Acetic acid, acetate, and valeric acid. *Geochim. Cosmochim. Acta* **67**, 3645–3664.

Miller S. L. and Bada J. L. (1988) Submarine hot springs and the origin of life. *Nature* **334**, 609–611.

Miller S. L. and Smith-Magowan D. (1990) The thermodynamics of the Krebs cycle and related compounds. *J. Phys. Chem. Ref. Data* **19**, 1049–1073.

Orsi W. D., Edgcomb V. P., Christman G. D. and Biddle J. F. (2013) Gene expression in the deep biosphere. *Nature* **499**, 205–208.

Petersen J. M., Zielinski F. U., Pape T., Seifert R., Moraru C., Amann R., Hourdez S., Girguis P. R., Wankel S. D., Barbe V., Pelletier E., Fink D., Borowski C., Bach W. and Dubilier N. (2011) Hydrogen is an energy source for hydrothermal vent symbioses. *Nature* **476**, 176–180.

Povoledo D. and Vallentyne J. R. (1964) Thermal reaction kinetics of the glutamic acid–pyroglutamic acid system in water. *Geochim. Cosmochim. Acta* **28**, 731–734.

Proskurowski G., Lilley M. D., Seewald J. S., Fruh-Green G. L., Olson E. J., Lupton J. E., Sylva S. P. and Kelley D. S. (2008) Abiogenic hydrocarbon production at Lost City hydrothermal field. *Science* **319**, 604–607.

Rona P. A., Boström K., Laubier L. and Smith, Jr., K. L. (1983) Hydrothermal processes at seafloor spreading centers. In *Proceedings of a NATO Advanced Research Institute. Marine Sciences*. Plenum Press, New York, p. 796.

Russell M. J., Hall A. J., Boyce A. J. and Fallick A. E. (2005) 100th anniversary special paper: on hydrothermal convection systems and the emergence of life. *Econ. Geol.* **100**, 419–438.

Seewald J. S. (1994) Evidence for metastable equilibrium between hydrocarbons under hydrothermal conditions. *Nature* **370**, 285–287.

Seewald J. S. (2001) Aqueous geochemistry of low molecular weight hydrocarbons at elevated temperatures and pressures: constraints from mineral buffered laboratory experiments. *Geochim. Cosmochim. Acta* **65**, 1641–1664.

Seewald J. S., Zolotov M. Y. and McCollom T. (2006) Experimental investigation of single carbon compounds under hydrothermal conditions. *Geochim. Cosmochim. Acta* **70**, 446–460.

Seyfried W. E., Foustoukos D. I. and Allen D. E. (2004) Ultramafic-hosted hydrothermal systems at mid-ocean ridges: chemical and physical controls on pH, redox, and carbon reduction reactions, in Mid-Ocean Ridges: hydrothermal interactions between the lithosphere and oceans. *Geophys. Monogr. Ser.* **148**, 267–284.

Shock E. L. (1988) Organic acid metastability in sedimentary basins. *Geology* **16**, 886–890.

Shock E. L. (1990a) Do amino acids equilibrate in hydrothermal fluids? *Geochim. Cosmochim. Acta* **54**, 1185–1189.

Shock E. L. (1990b) Geochemical constraints on the origin of organic compounds in hydrothermal systems. *Origins Life Evol. Biosph.* **20**, 331–367.

Shock E. L. (1992) Stability of peptides in high-temperature aqueous solutions. *Geochim. Cosmochim. Acta* **56**, 3481–3491.

Shock E. L. (2005) Chemical environments of submarine hydrothermal systems. *Origins Life Evol. Biosph.* **22**, 67–107.

Shock E. L. and Canovas P. (2010) The potential for abiotic organic synthesis and biosynthesis at seafloor hydrothermal systems. *Geofluids* **10**, 161–192.

Shock E. L., Sassani D. C., Willis M. and Sverjensky D. A. (1997) Inorganic species in geologic fluids: Correlations among standard molalthermodynamic properties of aqueous ions and hydroxide complexes. *Geochim. Cosmochim. Acta* **61**, 907–950.

Sverjensky D. A., Shock E. L. and Helgeson H. C. (1997) Prediction of the thermodynamic thermodynamic properties of aqueous metal complexes to 1000°C and 5 kb. *Geochim. Cosmochim. Acta* **61**, 1359–1412.

Vallentyne J. R. (1964) Biogeochemistry of organic matter – II Thermal reation kinetics and transformation products of amino compounds. *Geochim. Cosmochim. Acta* **28**, 157–188.

Wankel S. D., Germanovich L. N., Lilley M. D., Genc G., DiPerna C. J., Bradley A. S., Olson E. J. and Girguis P. R. (2011) Influence of subsurface biosphere on geochemical fluxes from diffuse hydrothermal fluids. *Nat. Geosci.* **4**, 461–468.

White R. H. (1984) Hydrolytic stability of biomolecules at high temperatures and its implications for life at 250 degrees C. *Nature* **310**, 430–432.

Wilson H. and Cannon R. K. (1937) The glutamic acid-pyrrolidone carboxylic acid system. *J. Biol. Chem.* **119**, 309–331.

Wolery T. J. (1992) EQ3NR, A Computer Program for Geochemical Aqueous Speciation-Solubility Calculations: Theoretical Manual, User's Guide, and Related Documentation (Version 7.0). Lawrence Livermore National Laboratory.

Yang Z., Gould I. R., Williams L. B., Hartnett H. E. and Shock E. L. (2012) The central role of ketones in reversible and irreversible hydrothermal organic functional group transformations. *Geochim. Cosmochim. Acta* **98**, 48–65.

Ziemer S. P. and Woolley E. M. (2007) Thermodynamics of the first and second proton dissociations from aqueous L-aspartic acid and L-glutamic acid at temperatures from (278.15 to 393.15) K and at the pressure 0.35 MPa: apparent molar heat capacities and apparent molar volumes of zwitterionic, protonated cationic, and deprotonated anionic forms at molalities from (0.002 to 1.0) mol·kg^{-1}. *J. Chem. Thermodyn.* **39**, 645–666.

Associate editor: John Moreau